

Response to reviewers

First, we would like to thank the reviewers for their valuable time, efforts, and advice.

Response to reviewer #2:

1. “My main concern is that two of the three original reviewers requested comparisons with TCCON, and the authors have done so, but have not included this in the revised manuscript nor in the supplementary materials.”

“I agree that what you have plotted is not an apples-to-apples comparison. I would suggest that instead, you average the TCCON data during the 30 minute aircraft sampling times instead of simply taking mid-day averages. I also do not see the need for your additional 3-sigma filtering.”

We have provided the TCCON data comparisons in the supporting information section of the revised manuscript, which also include the averaged TCCON data within 30 min. of aircraft measurements. Please see below:

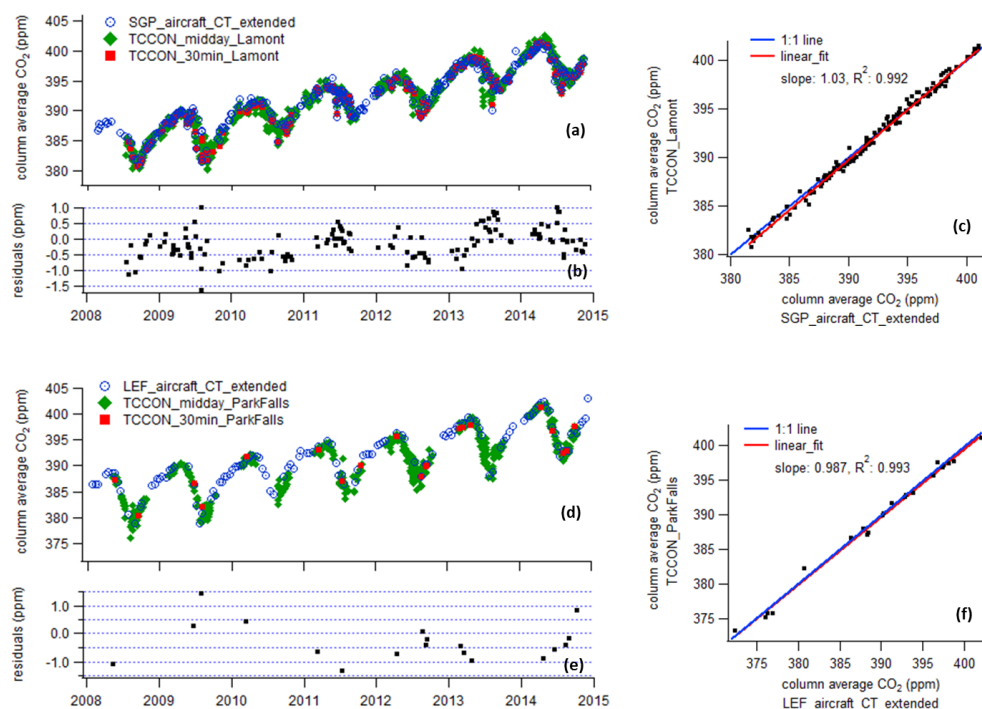


Fig. S2 Comparisons between aircraft and CT based total column CO₂ with TCCON total column CO₂. TCCON data with Solar Zenith Angle larger than 60° are not included in these comparisons. (a), (b), and (c) are time series, residuals (TCCON - aircraft_CT_extended), and

scatter plot comparisons between SGP and TCCON Lamont site (36.60⁰N, -97.49⁰E), respectively. (d), (e), and (f) are the same between LEF and TCCON Park Falls site (45.94⁰N, -90.27⁰E). In (a) and (d), TCCON midday values are the averages between 10:00 to 15:00 LST; TCCON 30 min. values are the averages within 30 min. of aircraft sampling time. TCCON 30 min. values are used in (b), (c), (e), and (f).

2. We stated in the previous response that "In addition, the aircraft and tower measurements are calibrated on WMO scale; however, direct calibrations of remote sensing instruments are not available. It makes more sense to compare TCCON against calibrated measurements for accuracy instead of the other way around. Our study focuses on the long-term mean spatial patterns of column CO₂ over North America and the influence of large-scale transport..."

Reviewer: "The overall scaling of the two data products is not of prime interest, here. As you mention, the long-term mean spatial pattern are primarily important, which I believe you can assess using a comparison with TCCON data. This might give you a way of assessing the CT stratosphere, and improving your product!"

We are not talking about overall (global) scaling, but those that depend on regional and seasonal conditions. We have evaluated the CT stratosphere simulations using calibrated measurements of AirCore, which shows reasonable agreements. However, TCCON data cannot be calibrated directly. That's why we opt to use AirCore for comparison.

3. We stated in the previous response that "For TCCON that sampling the whole column instantly at an angle, the actual sampling location, especially at high altitudes, may be far away from our aircraft inlets even though the distance on the ground is much smaller."

Reviewer: Near noon, this should be a less significant problem. At the very least, this is a quantifiable problem, and you have not demonstrated the problem in a quantitative manner. Also, you base much of your paper on the fact that the stratosphere does not change significantly in time or space, so this argument is not strong. (For example, you later state: "There is little spatial variation of atmospheric CO₂ in the stratosphere over mid-latitude region (Andrews et al., 2001)." and "We cannot properly assign an exact number as the uncertainty for the top 1/3 of the atmosphere without routine in-situ measurements. However, spatial gradient and atmospheric variability is very small in this part of the atmosphere, and thus it is not important in our study.")

The TCCON midday values are also provided in the revised manuscript. Our study focus on spatial gradients of the total column; as we can see from the Fig. 4d, Fig. 6, and Fig. 7, the spatial differences in the stratospheric CO₂ are very small compared with the tropospheric CO₂ (especially within the PBL). Thus, it is expected that the stratospheric CO₂ does not contribute significantly to the spatial differences of the total column.

Response to reviewer #3:

- The abstract makes this statement: “Our results confirm that continental-scale total column XCO₂ gradients simulated by CarbonTracker are realistic and can be used to evaluate the credibility of spatial patterns from satellite retrievals.

First, the authors only demonstrate that it is reliable in North America. No statements within the paper address why it should be reliable everywhere, considering that far more data are assimilated into CT from North America than anywhere else. The authors made such statements in the response to reviewers – these needed to be added to the paper to corroborate this claim.

- Line 434: Again the authors need to stress that CT is realistic over North America. Please rewrite to be: “Since spatial gradients from *CT2015* have been shown to be realistic on continental scales over North America, boreal fluxes inferred by CT2015 ... may be more trustworthy than....”

We have already answered this comment in the previous response. We admit that our study focuses on North America; however, our vigorous comparison between calibrated data and CT results has shown the significant influence of transport on column CO₂ gradients, and found smooth column CO₂ gradients. These conclusions should also apply in Europe. We don't think the transport over Western Europe can be so different from that over North America that it could explain the larger gradient and the hot spots in Reuter et al. (2014) Fig. 2. Our response was already provided (and copied here); the reviewer hasn't commented on our response:

“We think it is reasonable to believe that CT produces trustworthy results even outside North America, for the following reasons: (1) CT-Europe that simulate more surface measurements shows similar results as CT. (2) The transport in CT is reasonably well, supported by the good simulation of SF₆, a tracer for large-scale transport (see https://www.esrl.noaa.gov/gmd/ccgg/carbontracker/CT2016_doc.php#tth_sEc6, section 6.2). (3) The reviewer seems to suggest that we cannot judge the model performance in Europe because we don't have the truth to compare with, unlike the well-calibrated aircraft profiles we have in North America. But that's the case for all CO₂ models over Europe. At least for CT, it compared well with N.A. aircraft measurements, even though aircraft measurements are not assimilated in CT. This gives us more confidence for the CT model.”

In addition, CarbonTracker also shows reasonable agreement with TCCON sites in Europe (e.g. <https://www.esrl.noaa.gov/gmd/ccgg/carbontracker/tcon.php?site=bremen01>), and its performance is comparable with (or even better than some) other models (e.g. https://www.esrl.noaa.gov/gmd/ccgg/carbontracker/OCO2_insitu_rev1/tcon.php?ds=bremen&ruid=IS).

Second, the authors make no mention of potential sampling bias in the observations. In the case of their focus on the SCIAMACHY observations over Europe, section 3.5 still makes no mention of the possible sampling biases in the observations. The authors are sampling all data points over Europe all the time from their model. SCIAMACHY only makes measurements when it flies overhead, and when it is sufficiently clear (and this is true of all the CO₂-measuring sensors). When you average these irregular observations together, *you do not get a mean spatial pattern*. You get a mis-mash that includes whatever samples you happened to take. The authors need to mention this in the revised manuscript as a possible explanation of the appearance of an unphysical spatial pattern in the Reuter et al (2014) figure. How the data are used/assimilated is the critical factor. If the data are used ignoring this fact, it is of course a problem. But nearly all inversion systems sample the data at the times and places of the observations, so this effect is at least partially taken into account. Therefore, the claim in the abstract that CT can be used to evaluate mean spatial patterns from satellites is dubious, since *they are simply not the same thing*. The only way to get around this issue is to sample the model like the satellite, which the authors currently do not do nor discuss. For the paper to be acceptable, this statement in the abstract, and all related statements throughout the paper, needs to be either eliminated or qualified with this caveat.

The reviewer suggests that SCIAMACHY BESD (2003-2010 June-August) pattern in Reuter et al., 2014 is not a mean pattern (then Reuter et al., 2014 Fig. 2 is misleading to show this pattern as an 8-year statistics) and the sampling bias could be responsible for the unphysical column CO₂ pattern. We show here the data coverage of SCIAMACHY for 3 summers (2005/2006/2007), and the 3-year averaged column CO₂ pattern from sampling the CT2015 using SCIAMACHY latitude/longitude/date (see Figure below). SCIAMACHY retrievals provide good data coverage for most regions south of 55°N in Europe (except that United Kingdom and Ireland have less coverage). The averaged column CO₂ from CT2015 shows smaller gradients and smoother pattern, compared with SCIAMACHY BESD (Reuter et al., 2014 Fig. 2); this 3-year pattern already agrees with our understand of large-scale transport and meridional CO₂ gradients. Thus the sampling bias is unlikely the main reason for the large spatial difference of up to 6 ppm between Belgium, Netherland, north of Germany and south Ukraine and Kazakhstan in their figure. We are actually not sure on the specific causes for the unphysical pattern, thus we didn't commenting on this in our manuscript. But we will provide the above information regarding to the sampling bias in the revised manuscript and add the figure (d) in supporting material section. What we are sure about is that SCIAMACHY does not provide a credible spatial CO₂ pattern and we think it should be pointed out. The reviewer seems to be confirming that, in fact, SCIAMACHY's sampling biases prevent scientists from being able to infer reliable sources/sinks. We agree with that.

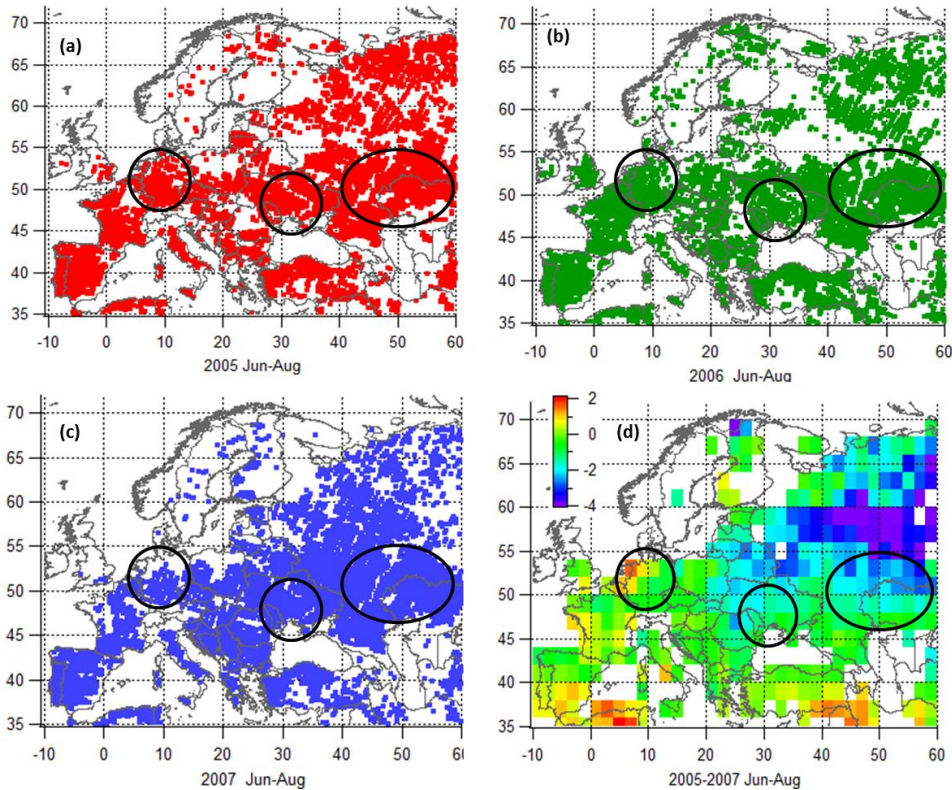


Figure for reviewing process. SCIAMACHY BESD data coverages for 2005 (a), 2006 (b), and 2007 (c) summer (JJA), and averaged (over three summers) column CO₂ pattern from sampling CT2015 with SCIAMACHY latitude/longitude/date for these periods (d). Black circles show the locations of extreme hot/cold spots with up to 6 ppm differences from Reuter et al. (2014), Fig.2. For (d), seasonal mean is first removed for each year before combining 3-year data together and averaged within a 2°×2° grid. Grids with less than 10 soundings for three summers are excluded; color scale shows maximum 6 ppm difference, similar as Reuter et al. (2014), Fig.2. SCIAMACHY latitude/longitude/date information is attained from http://www.esa-ghg-cci.org/sites/default/files/documents/public/documents/GHG-CCI_DATA.html. SCIAMACHY BESD data coverages for other years are accessible at: http://www.esa-ghg-cci.org/?q=webfm_send/200.

Then, the reviewer states that how the data are assimilated is a critical factor. If 8-year data still cannot provide realistic spatial gradients, then the inversion needs to be based on a priori assumptions and model transport, while a large portion of satellite measured radiances have to be ignored. We have already made this point in our previous response; however, the reviewer didn't comment on it. In the meantime one loses track of the evidence: (1) The influence of prior assumptions has to be tuned relative to the retrievals derived from the radiances. (2)The

assimilation process entrains transport biases of the transport models into the results. It is well established that all of these models have their own biases. That is why we are comparing the performance of CarbonTracker to calibrated aircraft and tower data, not to other transport models, nor to TCCON. Unlike the reviewer's statement about sampling the model like satellite, the "only way to get around the issue" of biases is to also compare other models and TCCON to calibrated data. They are the only data that stand on their own feet, no models needed.

- Regarding the comparison to TCCON, this comparison should at least be in the supplementary materials, along with error statistics. People have been comparing TCCON to aircraft for a long time and while it is not perfectly apples-to-apples, it can give a good idea of consistency. The authors saying "we don't need to do this" is unacceptable to this reviewer, considering they've already done it, they just need to include it.

We will provide the TCCON comparisons with aircraft + Carbon Tracker based column CO₂ in the supporting material:

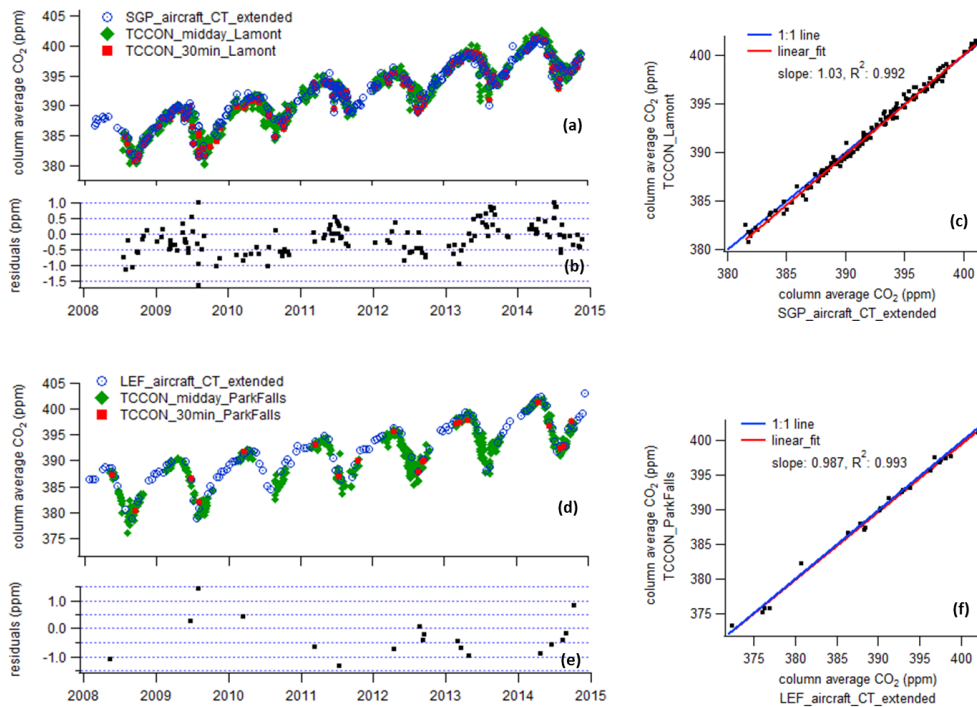


Fig. S2 Comparisons between aircraft and CT based total column CO₂ with TCCON total column CO₂. TCCON data with Solar Zenith Angle larger than 60° are not included in these comparisons. (a), (b), and (c) are time series, residuals (TCCON - aircraft_CT_extended), and scatter plot comparisons between SGP and TCCON Lamont site (36.60°N, -97.49°E),

respectively. (d), (e), and (f) are the same between LEF and TCCON Park Falls site (45.94⁰N, -90.27⁰E). In (a) and (d), TCCON midday values are the averages between 10:00 to 15:00 LST; TCCON 30 min. values are the averages within 30 min. of aircraft sampling time. TCCON 30 min. values are used in (b), (c), (e), and (f).

- Line 436: “However, the European carbon sink is still *elusive*”;

We will make the change in the revised paper.

Gradients of Column CO₂ across North America from the NOAA Global Greenhouse Gas Reference Network

Xin Lan^{1, 2}, Pieter Tans¹, Colm Sweeney^{1, 2}, Arlyn Andrews¹, Andrew Jacobson^{1, 2}, Molly Crotwell^{1, 2}, Edward Dlugokencky¹, Jonathan Kofler^{1, 2}, Patricia Lang¹, Kirk Thoning¹, Sonja Wolter^{1, 2}

¹National Oceanic and Atmospheric Administration, Earth System Research Laboratory, Boulder, 80303, Colorado, USA

²University of Colorado, Cooperative Institute for Research in Environmental Sciences, Boulder, 80309, Colorado, USA

Correspondence to: Xin.Lan (xin.lan@noaa.gov)

Abstract. This study analyzes seasonal and spatial patterns of column carbon dioxide (CO₂) over North America calculated from aircraft and tall tower measurements from the NOAA Global Greenhouse Gas Reference Network from 2004 to 2014. Consistent with expectations, gradients between the eight regions studied are larger below 2 km than above 5 km. The 11-year mean CO₂ dry mole fraction (XCO₂) in the column below ~330 hPa (~ 8 km above sea level) from NOAA's CO₂ data assimilation model, CarbonTracker (CT2015), demonstrates good agreement with those calculated from calibrated measurements on aircraft and towers. Total column XCO₂ was attained by combining modeled CO₂ above 330 hPa from CT2015 with the measurements. We find large spatial gradients of total column XCO₂ during June to August, with north and northeast regions having ~3 ppm stronger summer drawdown (peak to valley amplitude in seasonal cycle) than the south and southwest regions. The long-term averaged spatial gradients of total column XCO₂ across North America show a smooth pattern that mainly reflects the large-scale circulation. We have conducted a CarbonTracker experiment to investigate the impact of Eurasian long-range transport. The result suggests that the large summer time Eurasian boreal flux contributes about half of the north-south column XCO₂ gradient across North America. Our results confirm that continental-scale total column XCO₂ gradients simulated by CarbonTracker are realistic and can be used to evaluate the credibility of [some](#) spatial patterns from satellite retrievals, such as the long term average [of growing-season](#) spatial patterns from satellite retrievals reported for Europe which show larger spatial difference (~ 6 ppm) and scattered hot spots.

1 Introduction

Atmospheric measurements of carbon dioxide (CO₂) from ground and airborne platforms have greatly increased our knowledge of the global carbon cycle. Observations of CO₂, including the NOAA Global Greenhouse Gas Reference Network (GGGRN), initially emphasized ground-based measurements. These observations, started by C.D. Keeling, have monitored the CO₂ trend on both regional and global scales for over 50 years (e.g., Keeling and Rakestraw, 1960; Tans et al., 1989). In addition, the frequency and spatial distribution of airborne measurements have increased rapidly in the last two decades, providing important information about horizontal and vertical variability of atmospheric CO₂ (e.g., Gerbig et al., 2003; Choi et al., 2008; Biraud et al., 2013). Routine aircraft

36 measurements from the NOAA/ESRL GGRN monitor the large-scale distributions of a suite of trace gases,
37 including CO₂, under the influence of continental processes (Sweeney et al., 2015). A very successful approach has
38 been to employ commercial aircraft as a platform for CO₂ measurements, such as Japan's CONTRAIL
39 (Comprehensive Observation Network for TRace gases by AIrLiner) project, which has provided valuable
40 information for CO₂ in the high troposphere and lower stratosphere (Machida et al., 2002; Machida et al., 2008).
41 Vertical profiles of atmospheric CO₂ reflect the combined influences of surface fluxes and atmospheric mixing.
42 Vertical profiles are particularly useful for evaluating vertical mixing in atmospheric transport models that are used
43 for inverse modeling (e.g. Stephens et al., 2007) to derive estimates of regional- to continental-scale CO₂ sources
44 and sinks (e.g., Tans et al., 1990; Gurney et al., 2002; Gurney et al., 2004; Ciais et al., 2010;).

45 While CO₂ sources and sinks are well constrained at the global scale by global mass balance, it remains
46 challenging to accurately resolve CO₂ sources and sinks at regional to continental-scale, the apportionment of which
47 depends on relatively minor variations of the observed spatial and temporal patterns of CO₂. When averaging over a
48 few months and longer the largest portion of the variations over continents results from hemispheric-scale terrestrial
49 uptake/emissions (photosynthesis)/respiration) and fossil fuel emissions, while regional net fluxes can make a
50 relatively small contribution to the signal. For example, a simple mass balance argument shows that all U.S. CO₂
51 emissions from fossil fuel burning (~1.4 Pg yr⁻¹) create a total column enhancement of only 0.6 ppm on average in
52 air parcels over the East Coast compared to the West Coast and Gulf Coast if we assume an average residence time
53 of the emissions of 5 days for the winds to flush pass the contiguous U.S. (~8×10¹² m²).

54 With careful calibration, air handling, and analysis, the uncertainties of in-situ measurements are less than 0.1
55 ppm. However, in-situ observation networks are sparse in global and regional coverage. Remote sensing data
56 radically increase the number of observations and capture under-sampled regions. It could have a valuable impact on
57 our understanding of the carbon cycle. However, both the precision and the potential of even very small systematic
58 biases in remote sensing measurements need to be carefully evaluated, especially those that depend on regional and
59 seasonal conditions. Vertical profiles from in-situ CO₂ measurements have been used to evaluate ground-based total
60 column XCO₂ (the "X" stands for dry mole fraction) determinations, such as those from the Total Carbon Column
61 Observing Network (TCCON) (Washenfelder et al., 2006; Wunch et al., 2010; Messerschmidt et al., 2011; Tanaka
62 et al., 2012). The uncertainty of TCCON total column CO₂ is reported to be 0.4 ppm (1σ) after comparison to
63 aircraft measurements (Wunch et al., 2010). Vertical profiles are also used to evaluate other satellite retrievals of
64 total column XCO₂, such as those from the Tropospheric Emission Spectrometer (TES)(Kulawik et al., 2013) and
65 the Greenhouse Gases Observing SATellite (GOSAT) (Inoue et al., 2013, 2016; Saitoh et al., 2016). Satellite
66 retrieval products have known and unknown biases (due to errors in spectroscopy, viewing geometry, spatial
67 differences in clouds and aerosols, surface albedo, etc.) that can result in false horizontal gradients in total column
68 XCO₂ for inverse estimates of sources (Miller et al., 2007; Crisp et al., 2012; Feng et al., 2016). After correction for
69 known biases, the mean GOSAT total column CO₂ (NIES retrievals) biases range between -2.09 to 3.37 ppm (mean
70 = 0.11 ppm, S.D.= 1.11 ppm; 20 out of 27 stations show biases lower than 1 ppm) across different aircraft sites over
71 land when compared with aircraft-based total column XCO₂ (Inoue et al.,2016). The Orbiting Carbon Observatory-
72 2 (OCO-2) retrieval of total column XCO₂ was estimated to have a mean difference less than 0.5 ppm from TCCON,

73 with RMS differences typically below 1.5 ppm after bias correction (Wunch et al., 2016). The overall uncertainty of
74 satellite retrievals is relatively large compared with the total column XCO₂ calculated from in-situ measurements.
75 Total column XCO₂ calculated from vertical profiles from the Japanese CONTRAIL project (Machida et al., 2008)
76 and from the NOAA Carbon Cycle and Greenhouse Gas aircraft program (Sweeney et al., 2015) complemented with
77 simulated profiles from a chemistry–transport model above the maximum altitude of the data have uncertainty less
78 than 1 ppm (Miyamoto et al., 2013). The ~~relatively-smaller~~ uncertainty of the in situ-based total column XCO₂
79 suggests that they can be used to evaluate satellite retrievals of column averaged CO₂. Since aircraft profiles co-
80 located with satellite retrievals are rare, it is useful to consider the statistics of total column XCO₂ fields derived
81 from repeated aircraft profiles over particular locations.

82 The effect of satellite column averaging kernels and a priori profiles when comparing aircraft-based column
83 XCO₂ with GOSAT retrievals has been assessed by Inoue et al. (2013). For the case considered, application of the
84 averaging kernel and a priori profile to simulate total column XCO₂ was generally within ± 0.1 ppm of the density
85 weighted total column, suggesting that the averaging kernels can only account for small part of the overall
86 uncertainty of the GOSAT total column XCO₂ (Inoue et al., 2013).

87 Transparent and objective estimates of CO₂ sources and sinks derived from atmospheric measurements are
88 ~~essential paramount~~ for validating emissions reduction efforts and other mitigation policies, and for lowering the
89 uncertainties of carbon cycle-climate feedbacks. The latter are major ambiguities in predicting future climate, such
90 as potential uncontrolled CH₄ and CO₂ emissions from warming permafrost in Arctic regions. Satellite retrievals of
91 total column XCO₂ can significantly improve estimates of sources and sinks only if they are sufficiently precise and
92 accurate (Houweling et al., 2004; Chevallier et al., 2014), meaning that even very small systematic errors (biases)
93 must be eliminated. Here, we analyze the spatial and temporal variability of column CO₂ over North America using
94 well-calibrated CO₂ measurements from aircraft and tall tower, and we use model results from NOAA’s
95 CarbonTracker, version CT2015 (Peters et al. 2007, with updates documented at <http://carbontracker.noaa.gov>) to
96 investigate the primary drivers of variability in total column XCO₂. The aircraft data enable direct analysis of
97 column CO₂ characteristics, which is the fundamental step for accurate apportionment of sources and sinks. This
98 study focuses on ~~the~~ long-term averaged column CO₂ gradients and the contributions of different vertical layers to
99 the total column variability. It can serve as a reference for evaluating regional and seasonal biases of current and
100 future column CO₂ retrievals from both ground and satellite platforms.

101 2 Methods

102 2.1 Aircraft and tall tower sampling

103 Aircraft sampling in the NOAA GGGRN intends to provide vertical profiles of long-lived trace gases to capture
104 their seasonal and interannual variability. The aircraft sampling system consists of 12 borosilicate glass flasks in
105 each programmable flask package (PFP), a stainless-steel gas manifold system, and a data logging and control.
106 These flasks (0.7 L each) are pressurized to obtain 2.2 L of sample air from each target altitude. Air samples are then
107 shipped back to NOAA/ESRL for carefully calibrated and quality-controlled measurements. Carbon dioxide is

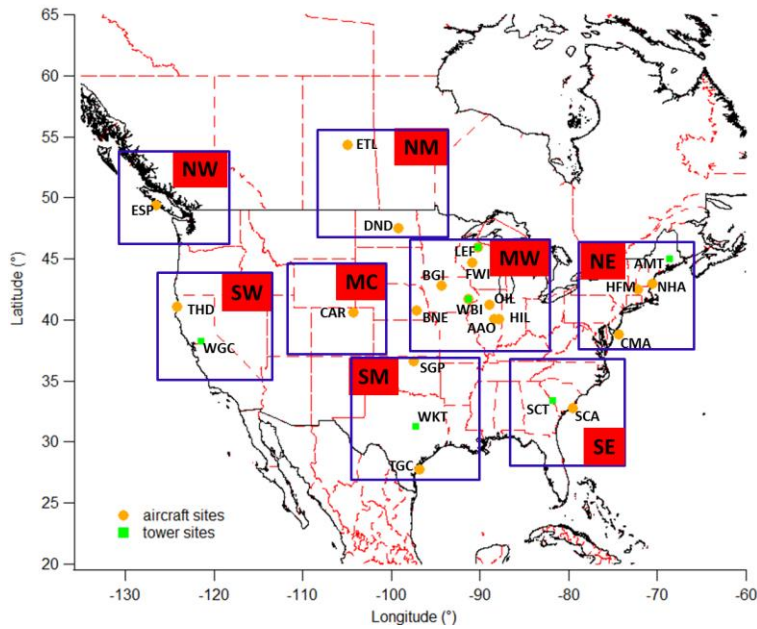
108 measured using a nondispersive infrared analyzer. Long-term measurements at ~15 sites are carried out using light
109 aircraft that can reach 8.5 km. Air samples are collected mostly during late morning to early afternoon, when the air
110 mass within the planetary boundary layer (PBL) is generally well mixed, and CO₂ enhancement near the ground
111 from plant respiration during the night has been mixed throughout the boundary layer. Normally, the aircraft follows
112 a pre-decided route such that most samples are collected within 0.1° of the site location. The sampling frequency
113 varies from site to site, currently from twice a month to once every 1.5 months. For more sampling details, quality
114 control discussions, and an evaluation of the sampling frequency, please refer to Sweeney et al. (2015). More
115 information on the aircraft sites can be found at <http://www.esrl.noaa.gov/gmd/ccgg/aircraft/>. We estimate the
116 uncertainty of individual measurements of CO₂ in flask air (68% confidence level) at 0.08 ppm. However, we have
117 seen evidence of positive biases for samples collected using older flasks that may contain contaminants. Andrews
118 et al. (2014) reported biases that increased from <0.1 ppm in 2008 to an average offset in 2013 of 0.36 ppm. The
119 aircraft sampling protocol was modified starting in August 2014 to mitigate this bias. For samples collected prior the
120 protocol change, laboratory tests showed that new/clean flasks have zero bias, but some older/dirty flasks could have
121 biases of > 1 ppm. This bias is not consistent among individual flasks and increasing over time (Andrews et al.,
122 2014), the potential bias is hard to quantify for measurements before August 2014. Thus, the high bias is not
123 corrected in our study. More recently, low bias has been found in PFP measurements when the ambient humidity is
124 high, based on comparisons of PFP measurements with data from in-situ analyzers at tall towers. We are working to
125 understand and quantify this bias, and for this study we have derived a preliminary correction factor, which shows a
126 linear trend with -1.4 ppm CO₂ offset per 1% above 1.7% of ambient water (mole fraction relative to whole air)
127 content. Only ~ 4% of total aircraft measurements or ~ 12% of those below 2 km are impacted by humidity higher
128 than 1.7%, for which we have applied corrections before data analysis. The mean correction applied is 0.53 ± 0.4 (1
129 σ) ppm for the impacted data.

130 The NOAA tall tower network measures CO₂ and other trace gases within the continental boundary layer.
131 Continuous in-situ measurements are conducted using nondispersive infrared (NDIR) absorption sensors and cavity
132 ring-down analyzers. The long-term stability of these systems is typically better than 0.1 ppm for CO₂ (Andrews et
133 al., 2014). Most tall tower sites have more than one air intake height. In this study, continuous in-situ measurements
134 from the highest intake are used to minimize potential influences from local sources. More information concerning
135 the tower sites can be found at <http://www.esrl.noaa.gov/gmd/ccgg/insitu/>. For the column XCO₂ calculation, tower
136 data only from 10:00-17:00 local standard time (LST) on flight days are averaged to one data point per day, as a
137 complement to vertical profiles within the PBL.

138 **2.2 Site description**

139 We analyze data from 19 aircraft sites and 6 tall tower sites during 2004 to 2014 (see Table S1 for a summary of site
140 conditions). After considering the geographic distribution of these sites in North America, we group them into eight
141 regions for spatial comparisons (Fig. 1). The northern west (NW) and southern west (SW) regions represent the
142 inflow area in the west coast of US, directly downwind of the Pacific Ocean at both higher elevations. The northern
143 mid-continent (NM) region represents the boreal forest and agriculture region in north-central North America. The

144 mid-continent (MC) region represents a dry landscape due to its high elevation (above 1.5 km on average) and semi-
 145 arid climate. The mid-west (MW) region is strongly influenced by agriculture and temperate forest. The southern
 146 mid-continent (SM) represents the south-central humid temperate region, with inflow from the Gulf of Mexico
 147 during summer. The northeast (NE) region represents the temperate forest in north-east coast of U.S., which is
 148 mostly downwind of regions to the west above the PBL, and downwind of its south-west regions within the PBL.
 149 The southeast (SE) region represents the warm temperate region in the south-east coast of U.S.
 150

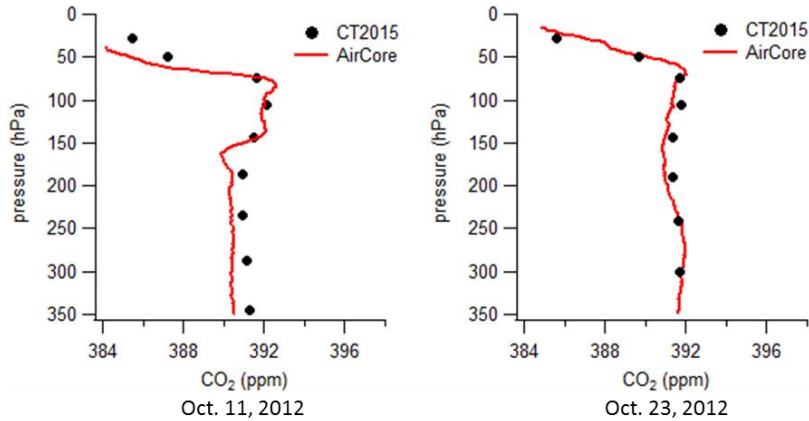


151
 152 **Fig. 1.** Aircraft, tall tower, and high elevation/tower sites in the NOAA GGRN. The eight boxes define regions
 153 that are further discussed for spatial pattern comparison.

154 **2.3 Smoothing of the reference data and column XCO₂ calculation**

155 We use Mauna Loa Observatory (MLO) as a reference site. ~~The long-term trend of CO₂ measurements from this~~
 156 ~~site is removed before combining multiple years of data to calculate long-term averages.~~ MLO is located at
 157 19.536°N, 155.576°W, and 3397 m above sea level. Carbon dioxide measurements from this site are widely used to
 158 represent background CO₂ in the Northern Hemisphere. For our study, a function consisting of a quadratic
 159 polynomial and four harmonics is fitted to the MLO data, adopted from the method described by Thoning et al.
 160 (1989). Residuals of the data from this function are smoothed by a low-pass filter with full-width at half-maximum
 161 in the time domain of 1.1 years. The smoothed residuals are then added back to the polynomial part of the function
 162 to produce the long-term deseasonalized trend. This trend (see Fig. 3) is subtracted from all aircraft and tall tower
 163 measurements. ~~Also, the , as well as from CarbonTracker model results (CarbonTracker - MLO deseasonalized~~

164 | ~~trend~~ CarbonTracker results presented in this study are the differences relative to observed MLO deseasonalized
165 trend. We use 'Δ' to represent detrended data in the following text and figures. The choice of reference site is not
166 important for this study, since we focus on examining the relative seasonal patterns of the detrended spatial and
167 vertical distributions of CO₂ instead of the total changes in CO₂ abundance attributed to global surface fluxes.
168



169
170 **Fig. 2.** Carbon Tracker (CT2015) simulations compared with AirCore in-situ measurements in upper atmosphere.
171 AirCore profiles in the left and right panels are sampled near CAR and SGP, respectively.
172

173 We calculate partial column average CO₂ dry mole fraction using tall tower and aircraft data, and the total
174 column by adding simulations of high altitude CO₂ (above 330 hPa, ~ 8 km above sea level) from CarbonTracker.
175 Since geometric height from the onboard Global Positioning System (GPS) (after 2006) or inferred from the aircraft
176 altimeter or pressure altitude is archived with each aircraft measurement, we first convert geometric height (in
177 meter) to pressure (in hPa) for the pressure-weighted column XCO₂ calculation. This conversion uses geopotential
178 data from NOAA/NCEP North American Regional Reanalysis (NARR) (Mesinger et. al, 2004), available at
179 <https://www.esrl.noaa.gov/psd/data/gridded/data.narr.html>, in which the geopotential is a function of latitude,
180 longitude, pressure altitude and time. We interpolate the geopotential field vertically to retrieve pressure, and then
181 calculate dry pressure by incorporating specific humidity data from NARR. Eventually we use a trapezoidal method
182 to integrate over detrended vertical profiles for dry-pressure-weighted column averages. For the long-term averaged
183 column ΔXCO₂ calculation, a long-term mean vertical profile is first constructed for each month by combining 11-
184 year detrended data together and then average data in each 40 hPa vertical bin. To look at the long-term averaged
185 total column ΔXCO₂ from individual aircraft sites, we combine aircraft data with upper-layer CT2015 simulations.

186 The NOAA CarbonTracker model assimilates CO₂ measurements from surface sampling networks and tall
187 towers to generate global 3D fields of atmospheric CO₂ mole fraction. The Carbon Tracker model has evolved
188 significantly since Peters et al. (2007). A detailed description of this model is provided in documents available at
189 <http://carbontracker.noaa.gov>. Our study utilizes CarbonTracker results from the 2015 release (CT2015), publicly

190 accessible at <ftp://aftp.cmdl.noaa.gov/products/carbontracker/co2/CT2015/molefractions/>. This version provides
191 CO₂ mole fraction over North America with 1° × 1° spatial and 3 hour temporal resolutions, which are analyzed in
192 Sect. 3.2 and 3.3. Total column CO₂ calculated from CT2015 global data with 3° × 2° spatial resolution is also
193 presented in the supporting information (SI). We have evaluated the performance of CarbonTracker in upper
194 atmosphere (330 to 0 hPa) by comparing its simulations with in-situ measurements from 9 AirCore profiles (Karion
195 et al., 2010) sampled in 2012-2014. AirCore is a ~150 m stainless steel tube that utilizes changes in ambient
196 pressure for passive sampling of the vertical profile. ~~The tube is carried to high altitude by It is released using~~
197 balloon and it collects a continuous sample as it descends. It is then measured by an analyzer after it is recovered.
198 More information about AirCore system can also be found at <https://www.esrl.noaa.gov/gmd/ccgg/aircore/>. All 9
199 AirCore profiles are taken near SGP and CAR sites. Figure 2 shows examples of AirCore profiles compared with
200 CT2015 in the upper atmosphere, which demonstrates good agreement. We also compare partial column (330 to 0
201 hPa) averages from the 9 AirCore profiles and CT2015. Results from CT2015 agree generally well with AirCore,
202 with difference ranging from 0.03 to 1.22 ppm (mean value equals 0.66 ppm), which suggests that CT2015 may
203 have a high bias that could contribute to 0.66×1/3=0.22 ppm overestimate on average to the total column average.
204 However, AirCore is in the process of rigorous evaluation, the differences between AirCore and CT2015 are not
205 well characterized yet since we only have a limited amount of AirCore data. It is unclear whether the potential bias
206 of CT2015 in this partial column is dependent on time or sampling location. Adding a constant bias correction to all
207 regions will not change the spatial gradients that we focus on in this study. Thus no correction is applied when using
208 CT2015 simulations to represent the upper 1/3 of the total column. For uncertainty estimates, we use a “bootstrap”
209 method that uses random resampling of individual vertical profiles with restitution (low bias, high humidity was
210 corrected), with 100 Monte Carlo runs for each column average calculation. Uncertainty is then defined as one
211 standard deviation of the 100 Monte Carlo results.

212 3 Results and Discussions

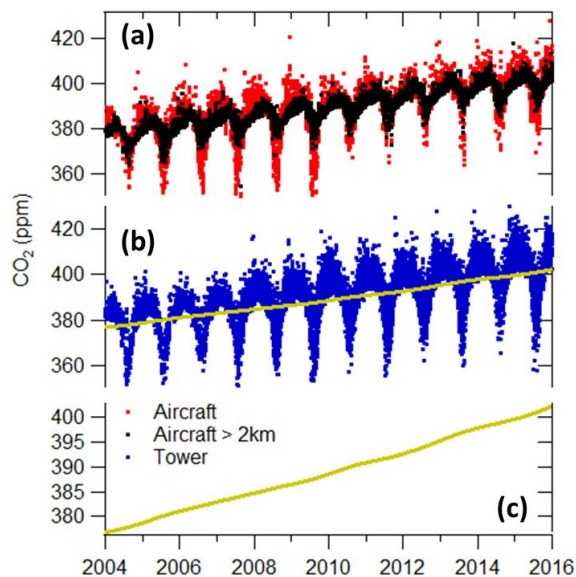
213 3.1 Seasonal patterns and spatial gradients

214 Typically one aircraft profile contains measurements at 12 different altitudes. Column ΔXCO_2 can be computed for
215 each profile using the method described in Sect. 2.3 (Fig. S1). Our aircraft and CT2015 based column CO₂ at SGP
216 and LEF sites shows reasonable agreements with TCCON data retrieved at Lamont and Park Falls site
217 (Washenfelder et al., 2006; Wunch et al. 2009, 2011), respectively (Fig. S2). Figure 3 shows aircraft (at all altitudes)
218 and tower data (daily averages for 10:00-17:00 LST data) from all sites used in this study. Aircraft data above 2 km
219 exhibit much smaller seasonal variations than the full dataset, because the variations are mainly driven by CO₂
220 sources and sinks near Earth’s surface. CO₂ mole fraction is enhanced in the shallow wintertime PBL primarily due
221 to reduced plant photosynthesis and ecosystem respiration combined with slightly increased fossil fuel emissions.
222 During summer the PBL is deeper, and depletions within the PBL are due to strong terrestrial uptake that dominates
223 over emissions especially during June through August. During summer of 2010 to 2012, CO₂ from aircraft
224 measurements appears higher than other years in Fig.3; however, similar characteristics are not present in tower

Formatted: Normal

225 | data. This **apparent** difference is due to a decrease in sampling frequency at several aircraft sites that resulted in an
226 | aliased picture of the full summer signals. Since we focus on climatological mean of 11 years of data in our study,
227 | this influence is eliminated by combining 11 years of data together into one “average year”.

Formatted: Font: Times, English (U.S.)



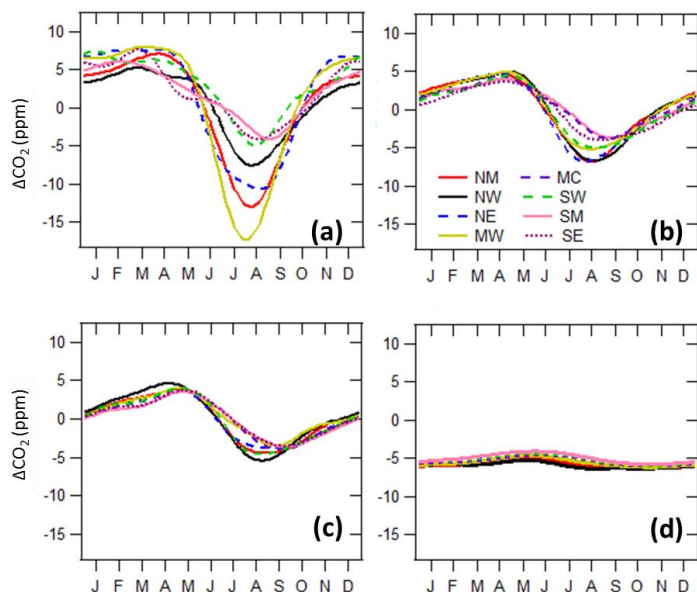
228 |
229 | **Fig. 3.** CO₂ observations from aircraft (a) and towers (b). The yellow line in (b) illustrates the deseasonalized trend
230 | at Mauna Loa (MLO), same as in (c), in which y-axis is expanded.

231 |
232 | To investigate the contributions of different altitudes to spatial gradients between regions, we divided all
233 | measurement data into three layers according to their sampling altitudes: below 2 km, 2 - 5km, and 5 - 8.5 km masl
234 | (Fig. 4). Smooth seasonal curves are attained from fitting data with four harmonics using the method described by
235 | Thoning et al. (1989). The peak-to-valley amplitudes of the seasonal cycles below 2 km are the largest among the
236 | three layers for most regions, with a minimum of 10.3 ppm in SM and a maximum of 25.0 ppm in MW. The
237 | seasonal variation amplitudes decrease to 7.7-11.5 ppm in the 2 - 5 km layer, and further decrease to 7.2-10.0 ppm
238 | in the 5 - 8.5 km layer. We also observe that the seasonal cycle drawdown occurs later in the layers above 2 km (see
239 | Fig. S32, which provides similar information as Fig. 4, but seasonal curves from different vertical layers are grouped
240 | by regions to facilitate comparisons of the phases of seasonal cycles). The seasonal CO₂ drawdown below 2 km is
241 | mainly influenced by terrestrial photosynthesis and gradients are **due to influenced by** local to regional fluxes, with
242 | an earlier onset of drawdown in southern regions than in northern regions. The seasonal cycle aloft is damped and
243 | lagged compared to the PBL, with influences from throughout the Northern Hemisphere and with spatial gradients
244 | likely driven by large-scale transport. The NW, SW, SM, and SE inflow regions have significant delays of more

245 than one month in the 2 - 5 km layer compared with the surface layer, which is likely due to the delayed phase of the
246 seasonal cycle in well-mixed air coming from the oceans. Vertical homogeneity of air over ocean was observed
247 during the HIAPER Pole-to-Pole Observations (HIPPO) aircraft campaign (Wofsy et al., 2011; Frankenberg et al.,
248 2016). As air masses are transported further inland, we observe reduced discrepancies of the timing of CO₂
249 drawdown between surface and upper layer air (2-5 km), which may be associated with the increased influence of
250 the land surface in the mid-troposphere due to strong convection over land. CO₂ drawdown in the 5 - 8.5 km layers
251 also occurs later than in the 2 - 5 km layers in most regions; however, differences between these two layers are
252 small. The declining amplitude and delayed phase of the seasonal cycle with altitude have been noted often (e.g.,
253 Tanaka et al., 1983; Ramonet et al., 2002; Gerbig et al., 2003, Sweeney et al. 2015). It demonstrates that there is lot
254 of important information in the vertical profile that is diminished in observations of the total column.

255 We find that the largest horizontal spatial gradients between regions occur below 2 km during summer time
256 (Fig. 4), with a maximum difference of ~15.5 ppm between MW and SM. SM and SW exhibit less pronounced
257 seasonal cycles, which is likely associated with air masses from the Gulf of Mexico and the Pacific Ocean,
258 respectively, whereas MW exhibits a deep summer drawdown (amplitude in seasonal cycles) partially as a result of
259 strong regional forest and crop uptake. Crevoisier et al. (2010) estimated the surface flux over North America using
260 vertical CO₂ measurements and average wind vectors, and reported that annually averaged land carbon fluxes in the
261 western (including SW region) and southern regions (including SM region) were neutral. The SE region also
262 demonstrates a less pronounced seasonal cycle with higher summertime levels compared with other northern
263 regions, which may be due to the sea-breeze influence in summer within PBL. In wintertime, CO₂ levels in NE and
264 MW are higher than in other regions, which result from regional fossil fuel and terrestrial biogenic emissions
265 combined with transport from the west and south.

266 Higher altitude data (above 2 km) exhibit only small spatial gradients. In the 2 - 5 km layer, the largest gradient
267 is 4 ppm in summer (Fig. 4b). It further decreases to less than 3 ppm in the 5 - 8.5 km layer (Fig. 4c). Figure 4d
268 shows modeled CO₂ mole fractions from CT2015 for the upper troposphere and above (330 hPa to 0 hPa), which are
269 used to fill in above the aircraft profiles for calculation of total column ΔXCO_2 . Spatial gradients in this layer are
270 less than 0.5 ppm, suggesting that the top third of the total column has little contribution to the spatial gradients of
271 the total column.



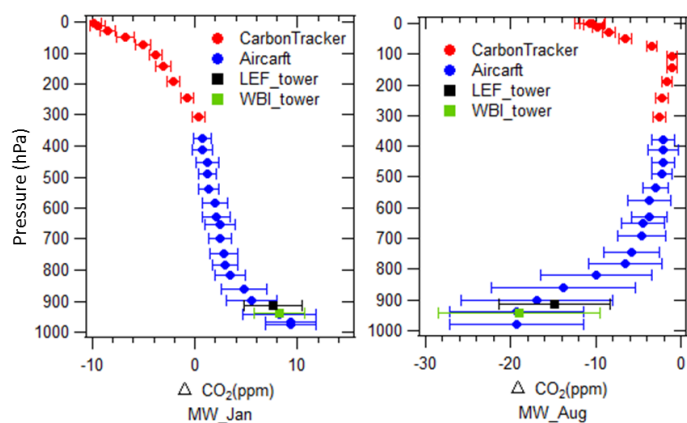
272
 273 **Fig. 4.** Multi-year (2004-2014) average smooth seasonal curves of CO₂ relative to the long-term de-seasonalized
 274 trend at Mauna Loa for different vertical layers: (a). Aircraft and tower data under 2 km, MC is not presented
 275 because only limited data were available due to high surface elevations (>1.5 km on average) in this region; (b).
 276 Aircraft data from 2 - 5 km; (c). Aircraft data from 5 - 8.5 km; (d). CT2015 model results for layers above 330 hPa
 277 (~8.5 km) to 0 hPa (~80 km).

278 3.2 Long-term mean vertical profiles

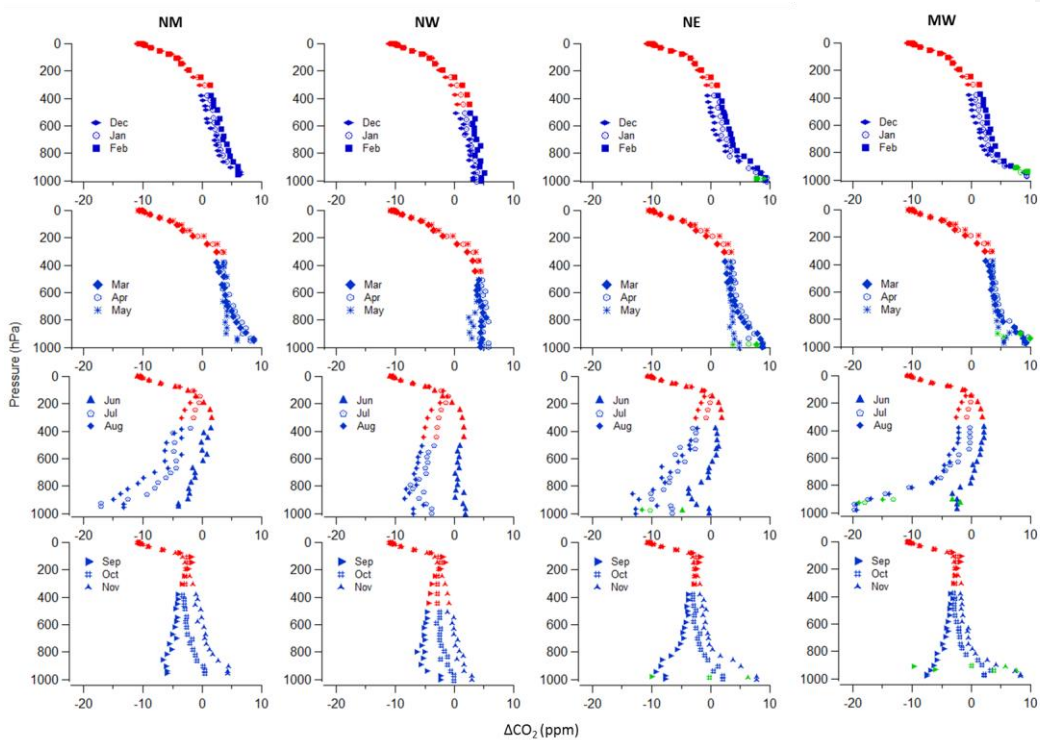
279 To investigate the mean spatial gradients, we first calculate the long-term mean monthly vertical profiles as
 280 described in Sect. 2.3. In addition, each tower serves as one additional layer in the mean profile. The long-term
 281 mean tower data generally fit well in the vertical profiles from measurements of aircraft samples (Fig. 5 and Fig. 6),
 282 suggesting that the biases described in Sect. 2.1 above do not significantly affect the long-term mean. To attain
 283 profiles of the entire atmospheric column, upper layers (330 to 0 hPa) are filled in by CT2015, and the lowest data
 284 point of the measured profile is extended to ground level, defined by the mean surface elevation in that region.

285 Figure 5 presents two examples of long term mean profiles with data variability, which is the one standard
 286 deviation for each 40 hPa bin of aircraft data or for all flight-day tower data. Variability as large as 20 ppm is seen
 287 within the PBL in the MW region in summer, which is due to strong and heterogeneous surface vegetation uptake
 288 and ecosystem respiration combined with day-to-day changes in wind direction. All long-term mean monthly
 289 vertical profiles are presented in Fig. 6, which shows the mean temporal and vertical variability of CO₂ in each
 290 season, and further demonstrates the vertical propagation of seasonal CO₂ due to changes of surface flux. In

291 wintertime, monotonic decrease of CO₂ with altitude can be observed from all regions, in which high PBL CO₂ is
 292 mainly driven by surface emissions and reduced vertical mixing (Denning et al., 1998; Stephens et al., 2007).
 293 Surface CO₂ decreases dramatically in the growing season in those regions influenced by high plant activity, such as
 294 NM and MW regions. For the summer vertical profiles in NE and SE region (east coast of the U.S.), the CO₂ mixing
 295 ratio is elevated in the layer under 900 hPa followed by significant decreases in upper layers until 750 hPa, and then
 296 increases with altitude until tropopause (Fig. 6). This is likely a result of sea breeze influence. Lower-troposphere air
 297 from the sea, lacking terrestrial uptake of CO₂, typically has higher CO₂ in summer compared with inland air.
 298 Polluted air previously advected offshore can be brought back along with sea breeze. Without significant vertical
 299 mixing over the marine surface, high levels of pollutants remain in those air masses. The convergence of sea breeze
 300 with prevailing wind moving offshore may create a period with a stalled frontal structure that can aggregate air
 301 pollutants (Banta et al., 2005). The convective internal boundary layer structure of the sea breeze system can
 302 significantly reduce mixing height (Miller et al., 2003), and also induces higher CO₂ levels. When the sea breeze is
 303 not dominant, air advected from southwest and west (the land) can also bring in polluted air with high CO₂ since this
 304 region is downwind of continental U.S. emissions (Miller et al., 2012).

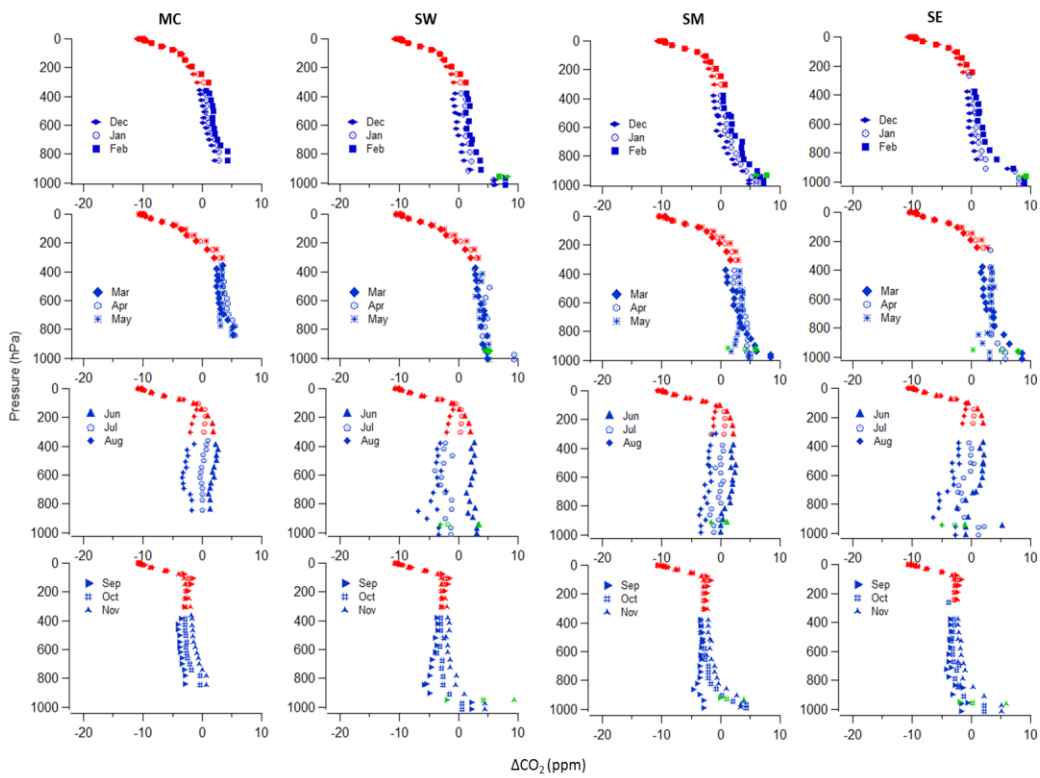


305
 306 **Fig. 5.** Long-term mean (2004-2014) average vertical profiles in January (left panel) and August (right panel) in
 307 region MW. Error bar shows one standard deviation.



308

309 **Fig. 6a.** Long-term mean (2004-2014) monthly vertical profiles in NM, NW, NE, MW (by column, from left to
 310 right). Blue points were calculated from observations, red points were calculated from CT2015, and green points
 311 were calculated from tower data.



312

313 **Fig. 6b.** Long-term mean (2004–2014) monthly vertical profiles in MC, SW, SM, SE (by column, from left to right).

314 Blue points were calculated from observations, red points were calculated from CT2015, and green points were

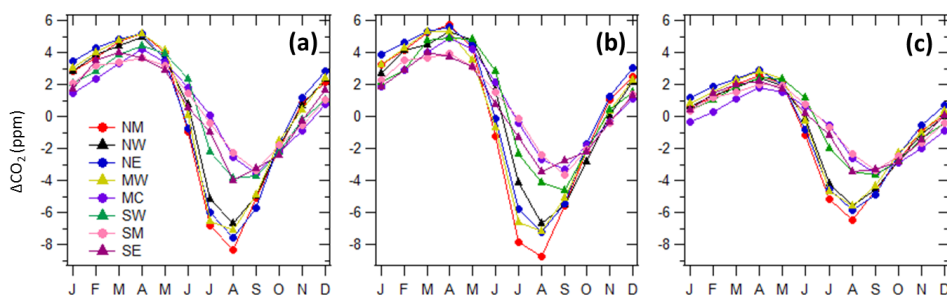
315 calculated from tower data.

316

317 **3.3 Partial column ΔXCO_2 and total column ΔXCO_2**

318 Seasonal variations of monthly averaged partial column ΔXCO_2 (below 330 hPa) demonstrate maximum values in
 319 April and minimum values in August or September (Fig. 7a). The largest amplitude appears in NM, with peak-to-
 320 valley difference up to 13.5 ppm. SW, SM, SE, and MC have similar amplitudes of 7-8 ppm, smaller than the other
 321 three regions. To evaluate the performance of CT2015 on column ΔXCO_2 , CT2015 results are sampled to match the
 322 latitude, longitude, altitude and time of actual measurements. Note that aircraft profiles are not assimilated in
 323 CT2015, so aircraft data are independent of the CT2015 data assimilation. Figure 7b shows monthly partial columns
 324 of ΔXCO_2 calculated from CT2015, which demonstrate good agreement with results from measurements. Only
 325 small seasonal biases exist in CT2015, with high bias occurring mostly in spring and early summer and low bias in
 326 September and October (Fig. S43). The overall differences of monthly partial column ΔXCO_2 (CT2015 -
 327 measurements) mainly fall in the range of -0.64 ppm (5th percentile) to 0.84 ppm (95th percentile) with a mean
 328 difference of 0.13 ppm. These differences are of similar magnitude to the uncertainties of partial column ΔXCO_2
 329 calculated from the measurements (Fig. S54). It is clear that CT2015 captures the long-term mean variations of both
 330 phase and amplitude of partial column XCO_2 reasonably well when compared with well-calibrated measurements
 331 across North America.

332



333

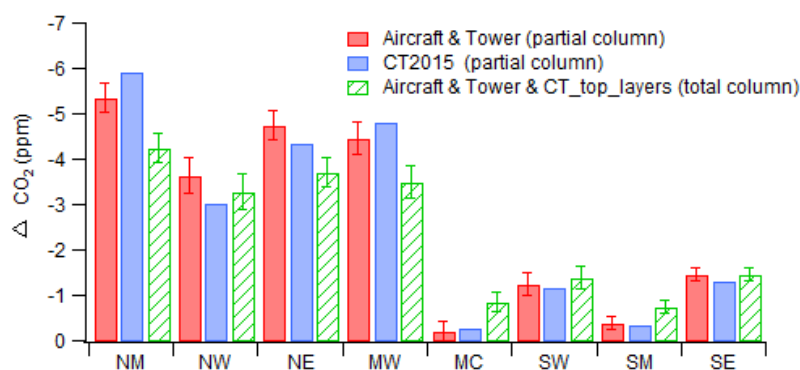
334 **Fig. 7.** (a). Partial column ΔXCO_2 calculated from aircraft and tower data; (b). Partial column ΔXCO_2 calculated
 335 from CT2015; (c). Total column ΔXCO_2 calculated from aircraft and tower data and including the top layer data
 336 from CT2015.

337

338 Total column ΔXCO_2 is presented in Fig. 7c. In regions NW, NM, NE, and MW, seasonal variations of total
 339 column ΔXCO_2 are very similar in both phase and amplitude (8-9 ppm peak to valley). For SW, SM, SE, and MC,
 340 amplitudes are ~5.5 ppm. The smallest spatial gradients occur during May and October, which result in maximum
 341 differences among all regions of only 0.9 and 0.7 ppm, respectively. The largest spatial gradients occur during June,
 342 July and August, which result in maximum differences of 2.4, 4.5, and 4.1 ppm, respectively. It is interesting that the
 343 deepest seasonal drawdown is seen in region NM, not in region MW that encompasses the very intensive

344 agricultural activities in the U.S. mid-west, which suggest the possibility of strong upwind influence in the NM
 345 region. Transported signals have significant influences on total column ΔXCO_2 . The summer total column ΔXCO_2 ,
 346 represented by the June to August average from CT2015, has a magnitude that is similar to observations with
 347 differences no more than 1 ppm (Fig. 8). Based on the seasonal patterns of total column ΔXCO_2 (Fig. 7c) and the
 348 summer column ΔXCO_2 (Fig. 8), we can separate the eight regions into two groups. The group with NW, NM, NE,
 349 and MW, has ~3 ppm stronger drawdown (larger amplitude) than the group with SW, SM, SE, and MC. For winter
 350 total column ΔXCO_2 (December to February average), the maximum spatial difference is only 1.6 ppm, with the
 351 highest total column ΔXCO_2 of 1.2 ppm in NE and the lowest value of -0.3 ppm in MC.

352



353

354 **Fig. 8.** Long-term mean (2004-2014) June to August partial and total column ΔXCO_2 . Error bars represent one
 355 standard deviation from the bootstrap uncertainty calculation (see Sect. 2.3).

356

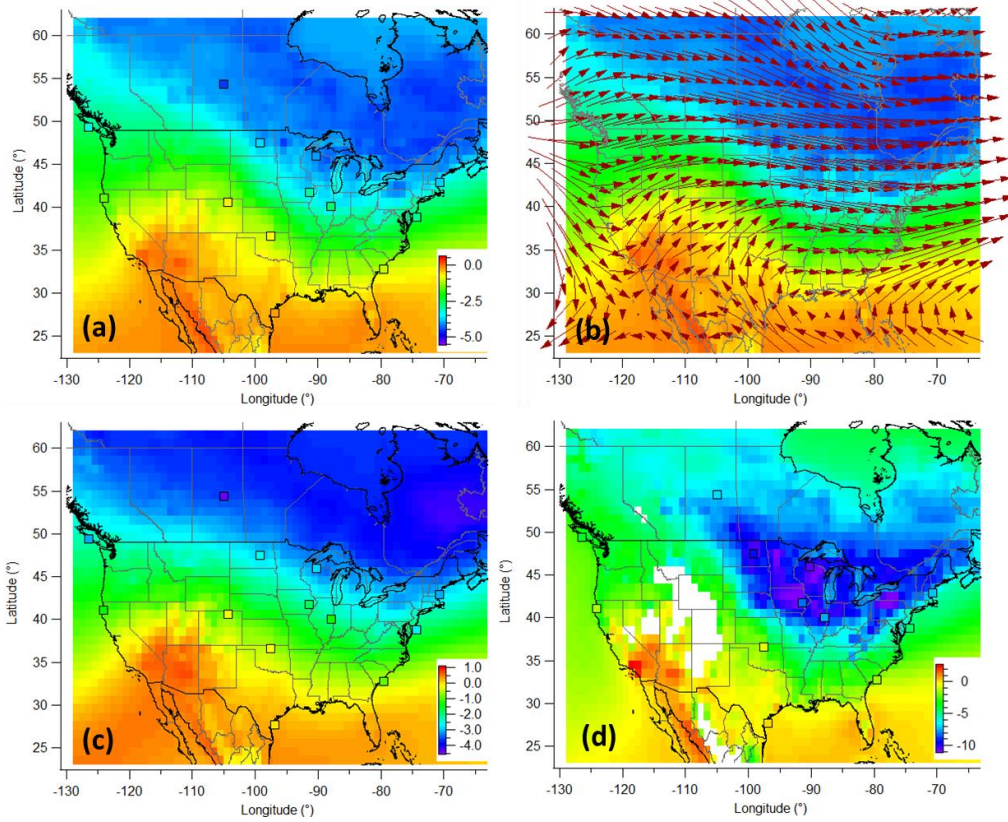
357 3.4 Influence of large scale circulation

358 Figure 9 shows long-term mean summer column ΔXCO_2 calculated from CT2015, together with full column
 359 ΔXCO_2 from individual aircraft sites. Note that some aircraft sites have less than 11 years of data that CT2015
 360 shows in Fig. 9, only aircraft sites with more than 6 years of data are presented, the actual values are provided in
 361 Table S2. The fact that total column ΔXCO_2 from CT2015 agrees well with aircraft sites supports the performance
 362 of CT2015 on a long-term average basis. The observations show a similar summer spatial pattern, with lower
 363 column ΔXCO_2 in the north and northeast regions and higher column ΔXCO_2 in the south and southwest regions
 364 (Fig. 9a). Scattered hot spots of high column ΔXCO_2 associated with surface emissions from megacities, or cold
 365 spots associated with strong local uptake, are not or just barely visible in the long-term average column ΔXCO_2 map
 366 at $1^\circ \times 1^\circ$ resolution. Instead, the wave-like pattern of column ΔXCO_2 over North America reflects the average large
 367 scale circulation. To support our hypothesis on the influence of large scale circulation, we analyze the long term
 368 mean wind pattern over North America. We can see that air masses from northwest of the continent bring in low
 369 average column ΔXCO_2 , while air masses from the south (mainly the subtropical Pacific Ocean and the Gulf of

370 Mexico) bring in high column ΔXCO_2 (Fig. 9b). The zonal gradients over the continent, especially north of 40° N,
371 also reflect long-term average wind patterns; southwest wind corresponds to higher column ΔXCO_2 over the western
372 part of the continent until the wind direction shifts to west-northwest over the eastern part of the continent. This
373 wind pattern matches well with the geographic division of the over/under -3 ppm areas colored in green/blue in the
374 column ΔXCO_2 map (Fig. 9b). Figure 9c and 9d shows partial column averages for free troposphere (800-330 hPa)
375 and lower troposphere (below 800 hPa), respectively. The free troposphere spatial gradient also demonstrates a
376 wave-like pattern. A previous study on the total column CO_2 from ground based Total Carbon Column Observation
377 Network (TCCON) found strong correlation between the mid-latitude column CO_2 and synoptic-scale variation of
378 potential temperature (θ , at 700 hPa), a dynamic tracer for adiabatic air transport (Keppel-Aleks et al., 2012). Thus
379 they also propose that the variations in column CO_2 are mainly driven by large-scale flux and transport. Analysis of
380 the interannual variability of the seasonal cycle amplitudes of column CO_2 in North Hemisphere has also found
381 significant contribution of large-scale circulations to the north-south gradient (Wunch et al., 2013).

382 The strong drawdown over northeast North America in summer is a consequence of long-range transport of low
383 CO_2 from northeast Eurasia, in addition to regional terrestrial uptake. Sweeney et al. (2015) notes well-mixed
384 vertical profiles (up to 8 km) of CO_2 , CO, CH_4 , N_2O , and SF_6 from THD, ESP and PFA (Poker Flat, Alaska; 65.07°,
385 -147.29°) sites and suggests that air coming across the Pacific was strongly influenced by Asian surface fluxes
386 before being vertically homogenized as it passed over the Pacific Ocean. This well-mixed air forms an important
387 boundary condition in the column CO_2 of air coming into the North American continent. This was best illustrated at
388 sites like PFA where the summertime minimum in CO_2 significantly preceded maximum ecosystem uptake of CO_2 ,
389 implying significant influence of transported air from lower latitude regions from Asia. We further conduct an
390 experiment using Carbon Tracker to investigate the importance of this effect. A control run and a “masked run” are
391 conducted for 2010-2012, in which the Eurasian boreal flux is turned on/off. The MLO CO_2 trend from each model
392 scenario is used as reference background and thus removed before total column ΔXCO_2 calculation. Figure 10 shows
393 the results for 2012 summer, which is an average summer when compared with the 2004-2014 mean pattern (Fig. 9
394 and Fig. 11). The maximum north-south difference reduces to ~2.5 ppm after we turn off the Eurasian boreal flux,
395 compared with ~5 ppm from the control run. In both control and masked scenarios, the free troposphere partial
396 ΔXCO_2 demonstrates similar spatial patterns as for total column ΔXCO_2 (Fig. S65). This result combined with
397 results from Sweeney et al. (2015) demonstrates that the transport of low CO_2 resulting from large summertime
398 Eurasian boreal uptake has a large contribution on the overall summer total column CO_2 decrease in North America.

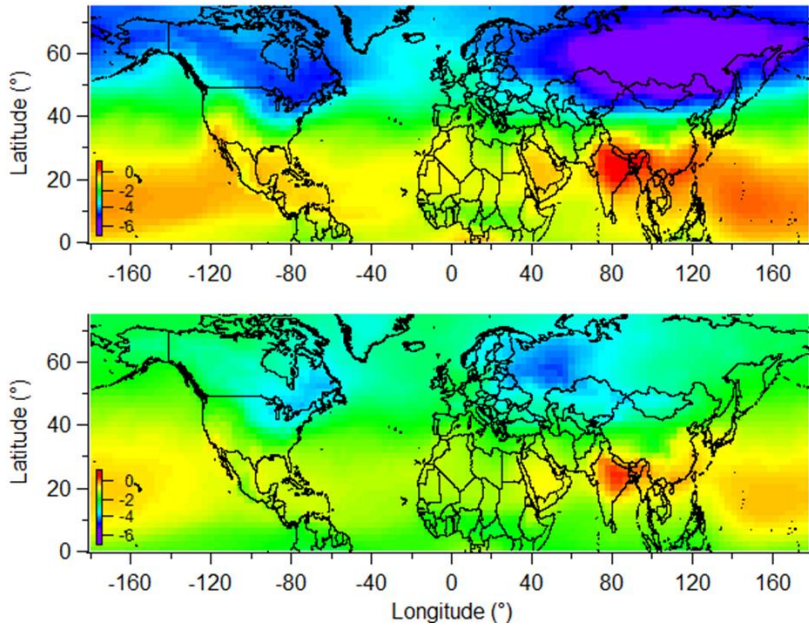
399
400



401

402 **Fig. 9.** Long-term mean (2004-2014) June-August total column ΔXCO_2 from CT2015 in $1^\circ \times 1^\circ$ spatial resolution
 403 with total column ΔXCO_2 for 13 individual aircraft sites in squares (a), and CT2015 column ΔXCO_2 overlaid with
 404 pressure-weighted (1000 hPa to 500 hPa) mean wind vectors for the same period (b). (c) and (d) are similar as (a),
 405 except for free troposphere (800 to 330 hPa) and lower troposphere (below 800 hPa), respectively. Note the different
 406 color scales.

407

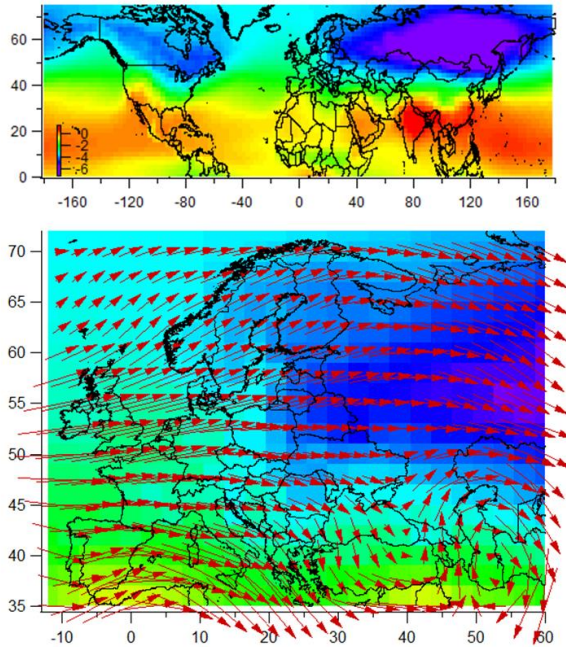


408
 409 **Fig. 10.** Total column ΔXCO_2 from Carbon Tracker control (top panel) and masked (bottom panel, Eurasian boreal
 410 flux is masked) runs for 2012 June–August ($3^\circ \times 2^\circ$ spatial resolution). MLO trend from each individual scenario is
 411 removed before the ΔXCO_2 calculation. Same color scale is used as in Fig. 9a. Partial column ΔXCO_2 patterns for
 412 free troposphere (800 to 330 hPa) and lower troposphere (below 800 hPa) are provided in SI.

413 3.5 A comparison with apparent gradients over Europe

414 Figure 11 shows the climatological June - August mean modeled global column ΔXCO_2 map in $3^\circ \times 2^\circ$ spatial
 415 resolution, which presents smooth wave-like patterns. Reuter et al. (2014) use SCIAMACHY and GOSAT satellite
 416 retrievals of column CO_2 and inverse modelling to infer a very large net ~~atmosphere~~ surface- CO_2 uptake flux over
 417 European region, and suggest a large uptake of CO_2 in this region. Column ΔXCO_2 from CT2015 (Fig. 11) exhibits
 418 a drastically different summer spatial pattern over Europe compared with the eight year mean (2003-2010) June
 419 through August satellite retrievals presented by Reuter et al. (2014, their Fig. 2a). The spatial gradient from CT2015
 420 results in a maximum 3-4 ppm difference and a gradual pattern, instead of as much as 6 ppm from satellite
 421 retrievals. There is no sign of XCO_2 hot spots from surface emissions or removals in the CT2015 spatial pattern over
 422 Europe (Fig. 11), in contrast to several hot spots that are apparent from the 8-year averaged SCIAMACHY satellite
 423 retrievals over Ireland, U.K., Belgium, Netherland, north of Germany, and south of Sweden, and low spots over the
 424 Ukraine and Kazakhstan (Reuter et al., 2014). The SCIAMACHY retrieval pattern contradicts our understanding of
 425 the significant influence of large-scale transport on column ΔXCO_2 . Although the NOAA/ESRL CT2015
 426 (<https://www.esrl.noaa.gov/gmd/ccgg/carbontracker/CT2015/>) assimilates fewer observations over Europe than

427 Carbon Tracker Europe (<http://www.carbontracker.eu/>), both models produced similar fluxes over the European
428 region (see both websites for detailed fluxes). The $3^{\circ} \times 2^{\circ}$ grid from CT2015 is not likely responsible for a much
429 smoother pattern for Carbon Tracker, compared with the $2^{\circ} \times 2^{\circ}$ grid from satellite retrievals (Reuter et al., 2014) .
430 The North America region on the $3^{\circ} \times 2^{\circ}$ grid in Fig. 11 shows similar pattern as the $1^{\circ} \times 1^{\circ}$ grid in Fig. 9, with
431 similar spatial difference of ~ 5 ppm. A smoother spatial distribution should be expected in Europe for the long-term
432 mean column XCO₂ (Fig. 11) due to the influences of dominating west and southwest winds in summer. We have
433 also evaluated the importance of sampling bias by sampling CT2015 at the same latitude/longitude/date as by
434 SCIAMACHY (Reuter et al., 2011). The 3-year (2005-2007) mean pattern shows much smaller gradients without
435 significant hot/cold spots at those locations as SCIAMACHY (Fig. S7). Sampling bias is unlikely the main reason
436 for the unphysical column XCO₂ spatial pattern from SCIAMACHY. Since the satellite retrievals in Reuter et al.
437 (2014) appear to show unrealistic column XCO₂ spatial gradients over Europe, they should not be used to derive any
438 estimates of a European carbon sink. A recent study (Feng et al., 2016) using inverse modeling suggests that satellite
439 retrievals outside the immediate European region and a small bias of only 0.5 ppm were sufficient to produce the
440 apparent large carbon sink in the study of Reuter et al. (2014). This is expected from elementary mass balance
441 considerations as in Sec.1 above. Spatial gradients are the fundamental signals to infer regional fluxes. Since spatial
442 gradients from CT2015 are realistic, boreal fluxes inferred by CT2015, which shows 0.03 ± 2.33 Pg C yr⁻¹ for
443 Europe, should be more trustworthy than fluxes estimated based on unrealistic spatial pattern. However, the
444 European carbon sink is still inconclusive; the discrepancies among different methods and results are further
445 discussed by Reuter et al. (2017). Increasing the amount of highly precise observations such as the well-calibrated
446 surface measurements and vertical profiles can greatly help to estimate the carbon sink.
447
448



449
 450 **Fig. 11.** Long-term mean (2004-2014) June - August total column ΔXCO_2 from CT2015 (top panel) in $3^\circ \times 2^\circ$
 451 spatial resolution, and detail for Europe overlaid with pressure-weighted (1000 hPa to 500 hPa) mean wind
 452 vectors for the same period (bottom panel). The color scale is the same as in Fig. 9a, which is scaled to reflect 6
 453 ppm difference of XCO_2 to compare with satellite retrievals from Reuter et al. (their Fig. 2a, 2014).

454 **4 Conclusion**

455 Aircraft and tall tower measurements from the NOAA GGGRN provide detailed information describing the long-
 456 term average temporal and spatial variations of CO_2 in the PBL and the free troposphere. These data provide
 457 valuable constraints for evaluating model simulations and satellite retrievals. Seasonal cycle peak-to-peak
 458 amplitudes of CO_2 are largest below 2 km, where those maximum values are about twice those in the vertical layers
 459 above, indicating that most of the information on surface sources and sinks resides in the continental PBL. Large
 460 spatial gradients of CO_2 over North America are observed below 2 km during summer (with maximum difference of
 461 ~ 15.5 ppm between MW and SM), while higher altitude data (above 2 km) have much smaller contributions to
 462 spatial gradients, with a maximum difference of 4 ppm. The spatial differences of CO_2 in the upper troposphere and
 463 above (330 hPa to 0 hPa) are less than 0.5 ppm, according to CT2015. Comparison with Aircore measurements
 464 shows CT2015 performs well simulating that the upper tropospheric and lower stratospheric patterns. simulations
 465 from CT2015 are reasonably trustworthy.

466 Our long-term mean vertical profiles show that tower data agree well with aircraft data at similar vertical levels.
467 Partial column ΔXCO_2 was calculated from the long-term mean vertical profiles. By comparing the partial column
468 ΔXCO_2 from measurements with those from CT2015, we verify that CT2015 captures the long-term mean patterns
469 of both phase and amplitude of partial ΔXCO_2 .

470 Large spatial gradients of ΔXCO_2 only appeared in summer, during which time the north and northeast regions
471 had ~ 3 ppm stronger drawdowns than the south and southwest regions. Scattered hot spots of high column ΔXCO_2
472 associated with surface emissions from megacities, or cold spots associated with strong local uptake, are not or just
473 barely visible in the long-term average column ΔXCO_2 . Instead, the wave-like pattern of column ΔXCO_2 over North
474 America matches well with the average large scale circulation. A CarbonTracker experiment to investigate the
475 impact of Eurasian long-range transport suggests that the large summer time Eurasian boreal flux alone contributes
476 about half of the north-south column ΔXCO_2 gradient across North America. Considering the transported signals
477 from other upwind regions, including northern Canada, we expect that the transported signals have the overall
478 largest contribution to the total column ΔXCO_2 spatial gradient.

479 **Author contributions**

480 Xin Lan was responsible for study design, data analysis, and manuscript writing. Pieter Tans was responsible for
481 study design, data analysis, and manuscript improvement. Colm Sweeney and Arlyn Andrews provided
482 measurement data and improved manuscript. Andrew Jacobson provided modelled data and improved manuscript.
483 Edward Dlugokencky analyzed measurements and ensured data quality, and improved manuscript. Jonathan Kofler
484 conducted tower measurements and improved manuscript. Molly Crotwell, Patricia Lang, and Sonja Wolter
485 analyzed measurements and ensured data quality. Kirk Thoning provided data smoothing method.

486 **Acknowledgements**

487 We especially thank John Mund for extracting NARR meteorological variables for our measurements. This
488 research was supported by a fellowship from the National Research Council Research Associateship Programs.

489 **References**

490 Andrews, A. E., Kofler, J. D., Trudeau, M. E., Williams, J. C., Neff, D. H., Masarie, K. A., Chao, D. Y., Kitzis, D.
491 R., Novelli, P. C., Zhao, C. L., Dlugokencky, E. J., Lang, P. M., Crotwell, M. J., Fischer, M. L., Parker, M. J.,
492 Lee, J. T., Baumann, D. D., Desai, A. R., Stanier, C. O., De Wekker, S. F. J., Wolfe, D. E., Munger, J. W. and
493 Tans, P. P.: CO₂, CO, and CH₄ measurements from tall towers in the NOAA Earth System Research
494 Laboratory's Global Greenhouse Gas Reference Network: instrumentation, uncertainty analysis, and
495 recommendations for future high-accuracy greenhouse gas monitoring efforts, *Atmos. Meas. Tech.*, 7, 647-687,
496 2014.

497 Banta, R. M., Senff, C. J., Nielsen-Gammon, J., Darby, L. S., Ryerson, T. B., Alvarez, R. J., Sandberg, S. R.,
498 Williams, E. J. and Trainer, M.: A bad air day in Houston', *B. Am. Meteorol. Soc.*, 86, 657, DOI:
499 <http://dx.doi.org/10.1175/BAMS-86-5-657>, 2005.

500 Biraud, S. C., Torn, M. S., Smith, J. R., Sweeney, C., Riley, W. J. and Tans, P. P.: A multi-year record of airborne
501 CO₂ observations in the US Southern Great Plains, *Atmos. Meas. Tech.*, 6, 751-763, 2013.

502 Buchwitz, M., Reuter, M., Bovensmann, H., Pillai, D., Heymann, J., Schneising, O., Rozanov, V., Krings, T.,
503 Burrows, J. P., Boesch, H., Gerbig, C., Meijer, Y. and Loscher, A. : Carbon Monitoring Satellite (CarbonSat):
504 assessment of atmospheric CO₂ and CH₄ retrieval errors by error parameterization, *Atmos. Meas. Tech.*, 6,
505 3477-3500, 2013.

506 Chevallier, F., Breon, F. M. and Rayner, P. J.: Contribution of the Orbiting Carbon Observatory to the estimation of
507 CO₂ sources and sinks: Theoretical study in a variational data assimilation framework, *J. Geophys. Res.*
508 *Atmos.*, 112, D09307, doi:10.1029/2006JD007375, 2007.

509 Choi, Y. H., Vay, S. A., Vadrevu, K. P., Soja, A. J., Woo, J. H., Nolf, S. R., Sachse, G. W., Diskin, G. S., Blake, D.
510 R., Blake, N. J., Singh, H. B., Avery, M. A., Fried, A., Pfister, L. and Fuelberg, H. E.: Characteristics of the
511 atmospheric CO₂ signal as observed over the conterminous United States during INTEX-NA, *J. Geophys. Res.*
512 *Atmos.*, 113, D07301, doi:10.1029/2007JD008899, 2008.

513 Ciais, P., Rayner, P., Chevallier, F., Bousquet, P., Logan, M., Peylin, P. and Ramonet, M.: Atmospheric inversions
514 for estimating CO₂ fluxes: methods and perspectives, *Climatic Change*, 103, 69-92, 2010.

515 Conway, T. J., Tans, P. P., Waterman, L. S. and Thoning, K. W.: Evidence for interannual variability of the carbon-
516 cycle from the national-oceanic-and-atmospheric-administration climate-monitoring-and-diagnostics-laboratory
517 global-air-sampling-network, *J. Geophys. Res. Atmos.*, 99, 22831-22855, 1994.

518 Crevoisier, C., Sweeney, C., Gloor, M., Sarmiento, J. L. and Tans, P. P.: Regional US carbon sinks from three-
519 dimensional atmospheric CO₂ sampling, *Proc. Natl. Acad. Sci. U. S. A.*, 107, 18348-18353, 2010.

520 Crisp, D., Fisher, B. M., O'Dell, C., Frankenberg, C., Basilio, R., Bosch, H., Brown, L. R., Castano, R., Connor, B.,
521 Deutscher, N. M., Eldering, A., Griffith, D., Gunson, M., Kuze, A., Mandrake, L., McDuffie, J.,
522 Messerschmidt, J., Miller, C. E., Morino, I., Natraj, V., Notholt, J., O'Brien, D. M., Oyafuso, F., Polonsky, I.,
523 Robinson, J., Salawitch, R., Sherlock, V., Smyth, M., Suto, H., Taylor, T. E., Thompson, D. R., Wennberg, P.
524 O., Wunch, D., and Yung, Y. L.: The ACOS CO₂ retrieval algorithm – Part II: Global XCO₂ data
525 characterization, *Atmos. Meas. Tech.*, 5, 687–707, doi:10.5194/amt-5-687-2012, 2012.

526 Dee, D. P., Uppala, S. M., Simmons, A. J., Berrisford, P., Poli, P., Kobayashi, S., Andrae, U., Balmaseda, M. A.,
527 Balsamo, G., Bauer, P., Bechtold, P., Beljaars, A. C. M., van de Berg, L., Bidlot, J., Bormann, N., Delsol, C.,
528 Dragani, R., Fuentes, M., Geer, A. J., Haimberger, L., Healy, S. B., Hersbach, H., Holm, E. V., Isaksen, L.,
529 Kallberg, P., Kohler, M., Matricardi, M., McNally, A. P., Monge-Sanz, B. M., Morcrette, J. J., Park, B. K.,
530 Peubey, C., de Rosnay, P., Tavolato, C., Thepaut, J. N. and Vitart, F.: The ERA-Interim reanalysis:
531 configuration and performance of the data assimilation system, *Q.J.R. Meteorol. Soc.*, 137, 553-597, 2011.

532 Denning, A. S., Takahashi, T., and Friedlingstein, P.: Can a strong atmospheric CO₂ rectifier effect be reconciled
533 with a “reasonable” carbon budget?, *Tellus B*, 51, 249–253, 1999.

534 Feng, L., Palmer, P. I., Parker, R. J., Deutscher, N. M., Feist, D. G., Kivi, R., Morino, I. and Sussmann, R.:
535 Estimates of European uptake of CO₂ inferred from GOSAT X-CO₂ retrievals: sensitivity to measurement bias
536 inside and outside Europe, *Atmos. Chem. Phys.*, 16, 1289-1302, 2016.

537 Frankenberg, C., Kulawik, S. S., Wofsy, S., Chevallier, F., Daube, B., Kort, E. A., O'Dell, C., Olsen, E. T., and
538 Osterman, G.: Using airborne HIAPER Pole-to-Pole Observations (HIPPO) to evaluate model and remote
539 sensing estimates of atmospheric carbon dioxide, *Atmos. Chem. Phys.*, 16, 7867–7878, 2016. doi:10.5194/acp-
540 16-7867-2016, 2016.

541 Gerbig, C., Lin, J. C., Wofsy, S. C., Daube, B. C., Andrews, A. E., Stephens, B. B., Bakwin, P. S. and Grainger, C.
542 A.: Toward constraining regional-scale fluxes of CO₂ with atmospheric observations over a continent: 1.
543 Observed spatial variability from airborne platforms *J. Geophys. Res. Atmos.*, 108, doi:10.1029/2002JD003018,
544 2003.

545 Chevallier, F., Palmer, P. I., Feng, L., Boesch, H., O'Dell, C. W., and Bousquet, P.: Towards robust and consistent
546 regional CO₂ flux estimates from in situ and space-borne measurements of atmospheric CO₂, *Geophys. Res.*
547 *Lett.*, 41, 1065–1070, doi:10.1002/2013GL058772, 2014.

548 Gourdji, S. M., Mueller, K. L., Yadav, V., Huntzinger, D. N., Andrews, A. E., Trudeau, M., Petron, G., Nehr Korn,
549 T., Eluszkiewicz, J., Henderson, J., Wen, D., Lin, J., Fischer, M., Sweeney, C. and Michalak, A. M.: North
550 American CO₂ exchange: inter-comparison of modeled estimates with results from a fine-scale atmospheric
551 inversion, *Biogeosci.*, 9, 457-475, 2012

552 Gurney, K. R., Law, R. M., Denning, A. S., Rayner, P. J., Baker, D., Bousquet, P., Bruhwiler, L., Chen, Y. H., Ciais,
553 P., Fan, S., Fung, I. Y., Gloor, M., Heimann, M., Higuchi, K., John, J., Maki, T., Maksyutov, S., Masarie, K.,
554 Peylin, P., Prather, M., Pak, B. C., Randerson, J., Sarmiento, J., Taguchi, S., Takahashi, T. and Yuen, C. W.:
555 Towards robust regional estimates of CO₂ sources and sinks using atmospheric transport models, *Nature*,
556 415(6872), 626-630, 2002.

557 Gurney, K. R., Law, R. M., Denning, A. S., Rayner, P. J., Pak, B. C., Baker, D., Bousquet, P., Bruhwiler, L., Chen,
558 Y. H., Ciais, P., Fung, I. Y., Heimann, M., John, J., Maki, T., Maksyutov, S., Peylin, P., Prather, M. and
559 Taguchi, S.: Transcom 3 inversion intercomparison: Model mean results for the estimation of seasonal carbon
560 sources and sinks, *Global Biogeochem. Cycles*, 18, GB1010, doi:10.1029/2003GB002111, 2004.

561 Houweling, S., Breon, F. M., Aben, I., Rodenbeck, C., Gloor, M., Heimann, M. and Ciais, P.: Inverse modeling of
562 CO₂ sources and sinks using satellite data: a synthetic inter-comparison of measurement techniques and their
563 performance as a function of space and time, *Atmos. Chem. Phys.*, 4, 523-538, 2004.

564 Inoue, M., Morino, I., Uchino, O., Miyamoto, Y., Yoshida, Y., Yokota, T., Machida, T., Sawa, Y., Matsueda, H.,
565 Sweeney, C., Tans, P. P., Andrews, A. E., Biraud, S. C., Tanaka, T., Kawakami, S. and Patra, P. K.: Validation
566 of XCO₂ derived from SWIR spectra of GOSAT TANSO-FTS with aircraft measurement data, *Atmos. Chem.*
567 *Phys.*, 13, 9771-9788, 2013.

568 Inoue, M., Morino, I., Uchino, O., Nakatsuru, T., Yoshida, Y., Yokota, T., Wunch, D., Wennberg, P. O., Roehl, C.
569 M., Griffith, D. W. T., Velazco, V. A., Deutscher, N. M., Warneke, T., Notholt, J., Robinson, J., Sherlock, V.,
570 Hase, F., Blumenstock, T., Rettinger, M., Sussmann, R., Kyrö, E., Kivi, R., Shiomi, K., Kawakami, S., De

571 Mazière, M., Arnold, S. G., Feist, D. G., Barrow, E. A., Barney, J., Dubey, M., Schneider, M., Iraci, L.,
572 Podolske, J. R., Hillyard, P., Machida, T., Sawa, Y., Tsuboi, K., Matsueda, H., Sweeney, C., Tans, P. P.,
573 Andrews, A. E., Biraud, S. C., Fukuyama, Y., Pittman, J. V., Kort, E. A., and Tanaka, T.: Bias corrections of
574 GOSAT SWIR XCO₂ and XCH₄ with TCCON data and their evaluation using aircraft measurement data,
575 *Atmos. Meas. Tech.* 9, 3491–3512, 2016, doi:10.5194/amt-9-3491-2016.

576 Karion, A., Sweeney, C., Tans, P., and Newberger, T.: AirCore: An Innovative Atmospheric Sampling System, *J.*
577 *Atmos. Ocean. Tech.*, 27, 1839–1853, doi:10.1175/2010JTECHA1448.1, 2010.

578 Karion, A., C. Sweeney, S. Wolter, T. Newberger, H. Chen, A. Andrews, J. Kofler, D. Neff, and P. Tans (2013),
579 Long-term greenhouse gas measurements from aircraft, *Atmos. Meas. Tech.*, 6(3), 511–526, doi:10.5194/amt-6-
580 511-2013.

581 Keeling, C. D. and Rakestraw, N. W.: The concentration of carbon dioxide in the atmosphere, *J. Geophys. Res.*, 65,
582 2502-2502, 1960.

583 Keppel-Aleks, G., Wennberg, P. O., Washenfelder, R. A., Wunch, D., Schneider, T., Toon, G. C., Andres, R. J.,
584 Blavier, J.-F., Connor, B., Davis, K. J., Desai, A. R., Messerschmidt, J., Notholt, J., Roehl, C. M., Sherlock, V.,
585 Stephens, B. B., Vay, S. A., and Wofsy, S. C.: The imprint of surface fluxes and transport on variations in total
586 column carbon dioxide, *Biogeosci.*, 9, 875–891, doi:10.5194/bg-9-875-2012, 2012.

587 Kulawik, S. S., Worden, J. R., Wofsy, S. C., Biraud, S. C., Nassar, R., Jones, D. B. A., Olsen, E. T., Jimenez, R.,
588 Park, S., Santoni, G. W., Daube, B. C., Pittman, J. V., Stephens, B. B., Kort, E. A., Osterman, G. B. and Team,
589 T. E. S.: Comparison of improved Aura Tropospheric Emission Spectrometer CO₂ with HIPPO and SGP
590 aircraft profile measurements, *Atmos. Chem. Phys.*, 13, 3205-3225, 2013.

591 Lauvaux, T., Schuh, A. E., Uliasz, M., Richardson, S., Miles, N., Andrews, A. E., Sweeney, C., Diaz, L. I., Martins,
592 D., Shepson, P. B. and Davis, K. J.: Constraining the CO₂ budget of the corn belt: exploring uncertainties from
593 the assumptions in a mesoscale inverse system, *Atmos. Chem. Phys.*, 12, 337-354, 2012.

594 Machida, T., Kita, K., Kondo, Y., Blake, D., Kawakami, S., Inoue, G. and Ogawa, T. : Vertical and meridional
595 distributions of the atmospheric CO₂ mixing ratio between northern midlatitudes and southern subtropics, *J.*
596 *Geophys. Res. Atmos.*, 108(D3), 8401, doi:10.1029/2001JD000910, 2002.

597 Machida, T., Matsueda, H., Sawa, Y., Nakagawa, Y., Hirotani, K., Kondo, N., Goto, K., Nakazawa, T., Ishikawa, K.
598 and Ogawa, T.: Worldwide Measurements of Atmospheric CO₂ and Other Trace Gas Species Using
599 Commercial Airlines, *J. Atmos. Ocean. Tech.*, 25(10), 1744-1754, 2008.

600 Mesinger, F., DiMego, G., Kalnay, E., Mitchell, K., Shafran, P. C., Ebisuzaki, W., Jovic, D., Woollen, J., Rogers,
601 E., Berbery, E. H., Ek, M. B., Fan, Y., Grumbine, R., Higgins, W., Li, H., Lin, Y., Manikin, G., Parrish, D., and
602 Shi, W.: North American regional reanalysis, *B. Am. Meteorol. Soc.*, 87, 343–360, doi:10.1175/BAMS-87-3-
603 343, 2006.

604 Messerschmidt, J., Geibel, M. C., Blumenstock, T., Chen, H., Deutscher, N. M., Engel, A., Feist, D. G., Gerbig, C.,
605 Gisi, M., Hase, F., Katrynski, K., Kolle, O., Lavric, J. V., Notholt, J., Palm, M., Ramonet, M., Rettinger, M.,
606 Schmidt, M., Sussmann, R., Toon, G. C., Truong, F., Warneke, T., Wennberg, P. O., Wunch, D. and Xueref-

607 Remy, I.: Calibration of TCCON column-averaged CO₂: the first aircraft campaign over European TCCON
608 sites, *Atmos. Chem. Phys.*, 11(21), 10765-10777, 2011.

609 Miller, C. E., Crisp, D., DeCola, P. L., Olsen, S. C., Randerson, J. T., Michalak, A. M., Alkhaled, A., Rayner, P.,
610 Jacob, D. J., Suntharalingam, P., Jones, D. B. A., Denning, A. S., Nicholls, M. E., Doney, S. C., Pawson, S.,
611 Boesch, H., Connor, B. J., Fung, I. Y., O'Brien, D., Salawitch, R. J., Sander, S. P., Sen, B., Tans, P., Toon, G.
612 C., Wennberg, P. O., Wofsy, S. C., Yung, Y. L. and Law, R. M.: Precision requirements for space-based X-CO₂
613 data, *J. Geophys. Res. Atmos.*, 112, D10314, doi:10.1029/2006JD007659, 2007.

614 Miller, J. B., Lehman, S. J., Montzka, S. A., Sweeney, C., Miller, B. R., Karion, A., Wolak, C., Dlugokencky, J.,
615 Southon, J., Turnbull, J. C., and Tans, P. P.: Linking emissions of fossil fuel CO₂ and other anthropogenic trace
616 gases using atmospheric ¹⁴CO₂, *J. Geophys. Res.*, 117, D08302, doi:10.1029/2011JD017048, 2012.

617 Miller, S. T. K., Keim, B. D., Talbot, R. W. and Mao, H.: Sea breeze: Structure, forecasting, and impacts, *Rev.*
618 *Geophys.*, 41, 1011, doi:10.1029/2003RG000124, 2003.

619 Miyamoto, Y., Inoue, M., Morino, I., Uchino, O., Yokota, T., Machida, T., Sawa, Y., Matsueda, H., Sweeney, C.,
620 Tans, P. P., Andrews, A. E. and Patra, P. K.: Atmospheric column-averaged mole fractions of carbon dioxide at
621 53 aircraft measurement sites, *Atmos. Chem. Phys.*, 13(10), 5265-5275, 2013.

622 Peters, W., Jacobson, A. R., Sweeney, C., Andrews, A. E., Conway, T. J., Masarie, K., Miller, J. B., Bruhwiler, L.
623 M. P., Petron, G., Hirsch, A. I., Worthy, D. E. J., van der Werf, G. R., Randerson, J. T., Wennberg, P. O., Krol,
624 M. C. and Tans, P. P.: An atmospheric perspective on North American carbon dioxide exchange:
625 CarbonTracker, *Proc. Natl. Acad. Sci. U. S. A.*, 104(48), 18925-18930, 2007.

626 Ramonet, M., Ciais, P., Nepomniachii, I., Sidorov, K., Neubert, R. E. M., Langendorfer, U., Picard, D., Kazan, V.,
627 Biraud, S., Gusti, M., Kolle, O., Schulze, E. D. and Lloyd, J.: Three years of aircraft-based trace gas
628 measurements over the Fyodorovskoye southern taiga forest, 300 km north-west of Moscow, *Tellus B-Chem.*
629 *Phys. Meteor.*, 54(5), 713-734, 2002.

630 Reuter, M., Bovensmann, H., Buchwitz, M., Burrows, J. P., Connor, B. J., Deutscher, N. M., Griffith, D. W. T.,
631 Heymann, J., Keppel-Aleks, G., Messerschmidt, J., Notholt, J., Petri, C., Robinson, J., Schneising, O., Sherlock,
632 V., Velasco, V., Warneke, T., Wennberg, P. O. and Wunch, D.: Retrieval of atmospheric CO₂ with enhanced
633 accuracy and precision from SCIAMACHY: Validation with FTS measurements and comparison with model
634 results, *J. Geophys. Res. Atmos.*, 116, 2011.

635 Reuter, M., Buchwitz, M., Hilker, M., Heymann, J., Schneising, O., Pillai, D., Bovensmann, H., Burrows, J. P.,
636 Bosch, H., Parker, R., Butz, A., Hasekamp, O., O'Dell, C. W., Yoshida, Y., Gerbig, C., Nehrkorn, T.,
637 Deutscher, N. M., Warneke, T., Notholt, J., Hase, F., Kivi, R., Sussmann, R., Machida, T., Matsueda, H. and
638 Sawa, Y.: Satellite-inferred European carbon sink larger than expected, *Atmos. Chem. Phys.*, 14(24), 13739-
639 13753, 2014.

640 Reuter, M., Buchwitz, M., Hilker, M., Heymann, J., Bovensmann, H., Burrows, J. P., Houweling, S., Liu, Y. Y.,
641 Nassar, F., Chevallier, F., Cias, P., Marshall, J., and Reichstein, M.: How much CO₂ is taken up by the
642 European terrestrial biosphere? *Bull. Am. Meteor. Soc.*, 98, 665-671, doi:10.1175/BAMS-D-15-00310.1, 2017.

643 Saitoh, N., Kimoto, S., Sugimura, R., Imasu, R., Kawakami, S., Shiomi, K., Kuze, A., Machida, T., Sawa, Y. and
644 Matsueda, H.: Algorithm update of the GOSAT/TANSO-FTS thermal infrared CO₂ product (version 1) and
645 validation of the UTLS CO₂ data using CONTRAIL measurements, *Atmos. Meas. Tech.*, 9(5), 2119-2134,
646 2016.

647 Stephens, B. B., Gurney, K. R., Tans, P. P., Sweeney, C., Peters, W., Bruhwiler, L., Ciais, P., Ramonet, M.,
648 Bousquet, P., Nakazawa, T., Aoki, S., Machida, T., Inoue, G., Vinnichenko, N., Lloyd, J., Jordan, A., Heimann,
649 M., Shibistova, O., Langenfelds, R. L., Steele, L. P., Francey, R. J. and Denning, A. S.: Weak northern and
650 strong tropical land carbon uptake from vertical profiles of atmospheric CO₂, *Science*, 316(5832), 1732-1735,
651 2007.

652 Sweeney, C., Karion, A., Wolter, S., Newberger, T., Guenther, D., Higgs, J. A., Andrews, A. E., Lang, P. M., Neff,
653 D., Dlugokencky, E., Miller, J. B., Montzka, S. A., Miller, B. R., Masarie, K. A., Biraud, S. C., Novelli, P. C.,
654 Crotwell, M., Crotwell, A. M., Thoning, K. and Tans, P. P.: Seasonal climatology of CO₂ across North America
655 from aircraft measurements in the NOAA/ESRL Global Greenhouse Gas Reference Network, *J. Geophys. Res.*
656 *Atmos.*, 120(10), 5155-5190, 2015.

657 Tanaka, M., Nakazawa, T. and Aoki, S.: Concentration of atmospheric carbon-dioxide over Japan, *J. Geophys. Res.*
658 *Ocean.*, 88(C2), 1339-1344, DOI: 10.1029/JC088iC02p01339, 1983.

659 Tanaka, T., Miyamoto, Y., Morino, I., Machida, T., Nagahama, T., Sawa, Y., Matsueda, H., Wunch, D., Kawakami,
660 S. and Uchino, O.: Aircraft measurements of carbon dioxide and methane for the calibration of ground-based
661 high-resolution Fourier Transform Spectrometers and a comparison to GOSAT data measured over Tsukuba
662 and Moshiri, *Atmos. Meas. Tech.*, 5(8), 2003-2012, 2012.

663 Tans, P. P., Conway, T. J. and Nakazawa, T.: Latitudinal distribution of the sources and sinks of atmospheric
664 carbon-dioxide derived from surface observations and an atmospheric transport model, *J. Geophys. Res.*
665 *Atmos.*, 94(D4), 5151-5172, 1989.

666 Tans, P. P., Fung, I. Y. and Takahashi, T.: Observational constraints on the global atmospheric CO₂ budget, *Science*,
667 247(4949), 1431-1438, 1990.

668 Thoning, K. W., Tans, P. P. and Komhyr, W. D.: Atmospheric carbon-dioxide at Mauna Loa observatory. 2.
669 Analysis of the NOAA GMCC data, 1974-1985, *J. Geophys. Res. Atmos.*, 94(D6), 8549-8565, 1989.

670 Washenfelder, R. A., Toon, G. C., Blavier, J. F., Yang, Z., Allen, N. T., Wennberg, P. O., Vay, S. A., Matross, D.
671 M. and Daube, B. C.: Carbon dioxide column abundances at the Wisconsin Tall Tower site, *J. Geophys. Res.*
672 *Atmos.*, 111, D22305, doi:10.1029/2006JD007154, 2006.

673 Wofsy, S. C.: HIPER Pole-to-Pole Observations (HIPPO): finegrained, global-scale measurements of climatically
674 important atmospheric gases and aerosols, *Philos. T. R. Soc. A*, 369, 2073-2086, doi:10.1098/rsta.2010.0313,
675 2011.

676 Wunch, D., Wennberg, P. O., Toon, G. C., Keppel-Aleks, G., and Yavin Y. G.: Emissions of greenhouse gases from
677 a North American megacity, *Geophys. Res. Lett.*, 36, L15810, doi:10.1029/2009GL039825, 2009.

678 Wunch, D., Toon, G. C., Wennberg, P. O., Wofsy, S. C., Stephens, B. B., Fischer, M. L., Uchino, O., Abshire, J. B.,
679 Bernath, P., Biraud, S. C., Blavier, J. F. L., Boone, C., Bowman, K. P., Browell, E. V., Campos, T., Connor, B.

680 J., Daube, B. C., Deutscher, N. M., Diao, M., Elkins, J. W., Gerbig, C., Gottlieb, E., Griffith, D. W. T., Hurst,
681 D. F., Jimenez, R., Keppel-Aleks, G., Kort, E. A., Macatangay, R., Machida, T., Matsueda, H., Moore, F.,
682 Morino, I., Park, S., Robinson, J., Roehl, C. M., Sawa, Y., Sherlock, V., Sweeney, C., Tanaka, T. and Zondlo,
683 M. A.: Calibration of the Total Carbon Column Observing Network using aircraft profile data', *Atmos. Meas.*
684 *Tech.*, 3(5), 1351-1362, 2010.

685 Wunch, D., Toon, G. C., Blavier, J.-F. L., Washenfelder, R. A., Notholt, J., Connor, B. J., Griffith, D. W. T.,
686 Sherlock, V., and Wennberg, P. O.: The total carbon column observing network, *Philosophical Transactions of*
687 *the Royal Society - Series A: Mathematical, Physical and Engineering Sciences*, 369(1943), 2087-2112,
688 doi:10.1098/rsta.2010.0240, 2011.

689 Wunch, D., Wennberg, P. O., Messerschmidt, J., Parazoo, N. C., Toon, G. C., Deutscher, N. M., Keppel-Aleks, G.,
690 Roehl, C. M., Randerson, J. T., Warneke, T., and Notholt, J.: The covariation of Northern Hemisphere
691 summertime CO₂ with surface temperature in boreal regions, *Atmos. Chem. Phys.*, 13, 9447-9459,
692 doi:10.5194/acp-13-9447-2013, 2013.